

Keck HIRES Spectroscopy of Extragalactic H II Regions: C and O Abundances from Recombination Lines¹

César Esteban

*Instituto de Astrofísica de Canarias, E-38200 La Laguna, Tenerife, Spain; and
Departamento de Astrofísica, Universidad de La Laguna, E-38071 La Laguna, Tenerife,
Spain*

cel@iac.es

Fabio Bresolin

Institute for Astronomy, 2680 Woodlawn Drive, Honolulu, HI 96822, USA

bresolin@ifh.hawaii.edu

Manuel Peimbert

Instituto de Astronomía, UNAM, Apdo. Postal 70-264, México 04510 D.F., Mexico

peimbert@astroscu.unam.mx

Jorge García-Rojas

Instituto de Astronomía, UNAM, Apdo. Postal 70-264, México 04510 D.F., Mexico

jgarcia@astroscu.unam.mx

Antonio Peimbert

Instituto de Astronomía, UNAM, Apdo. Postal 70-264, México 04510 D.F., Mexico

peimbert@astroscu.unam.mx

Adal Mesa-Delgado

Instituto de Astrofísica de Canarias, E-38200 La Laguna, Tenerife, Spain

amd@iac.es

ABSTRACT

We present very deep spectrophotometry of 14 bright extragalactic H II regions belonging to spiral, irregular, and blue compact galaxies. The data for 13 objects were taken with the HIRES echelle spectrograph on the Keck I telescope. We have measured C II recombination lines in 10 of the objects and O II recombination lines in 8 of them. We have determined electron temperatures from line ratios of several ions, specially of low ionization potential ones. We have found a rather tight linear empirical relation between $T_e([\text{N II}])$ and $T_e([\text{O III}])$. We have found that O II lines give always larger abundances than [O III] lines. Moreover, the difference of both O^{++} abundance determinations –the so-called abundance discrepancy factor– is very similar in all the objects, with a mean value of 0.26 ± 0.09 dex, independently of the properties of the H II region and of the parent galaxy. Using the observed recombination lines, we have determined the O, C, and C/O radial abundance gradients for 3 spiral galaxies: M 33, M 101, and NGC 2403, finding that C abundance gradients are always steeper than those of O, producing negative C/O gradients accross the galactic disks. This result is similar to that found in the Milky Way and has important implications for chemical evolution models and the nucleosynthesis of C.

Subject headings: galaxies: abundances –galaxies: individual (M 31, M 33, M 83, M 101, NGC 1741, NGC 2366, NGC 2403, NGC 4395, NGC 4861) – galaxies: ISM – galaxies: spiral – H II regions

1. Introduction

The spectral analysis of H II regions allows the determination of the chemical composition of the ionized gas-phase of the interstellar medium from the solar neighbourhood to the high-redshift Universe. Therefore, it stands as an essential tool for our knowledge of the chemical evolution of the Universe. With the advent of 8-10 m class ground-based telescopes, we can now obtain extremely deep spectra of extragalactic H II regions (hereafter EHRs). These new studies have permitted, for example, to obtain direct determinations of the electron temperature, T_e , in high-metallicity EHRs (see Bresolin 2008, and references therein),

¹Most of the data presented herein were obtained at the W.M. Keck Observatory, which is operated as a scientific partnership among the California Institute of Technology, the University of California and the National Aeronautics and Space Administration. The Observatory was made possible by the generous financial support of the W.M. Keck Foundation. Part of the observations were made with the 4.2 m William Herschel Telescope (WHT), operated on the island of La Palma by the Isaac Newton Group in the Spanish Observatorio del Roque de los Muchachos of the Instituto de Astrofísica de Canarias.

where the auroral lines become very faint, or to measure recombination lines (hereafter RLs) useful for abundance determinations of heavy-element ions (Peimbert 2003; López-Sánchez et al. 2007; Bresolin 2007).

The detection of C II and O II lines produced by pure recombination in EHRs was firstly reported by Esteban et al. (2002) from deep spectra taken with the 4.2 m William Herschel Telescope. In principle, these lines have the advantage that their intensity is much less dependent on the value of T_e than the collisionally excited lines (hereafter CELs), which are the lines commonly used for abundance determinations in nebulae. The brightest C II RL is C II $\lambda 4267$, with typical fluxes of the order of $10^{-3} \times I(\text{H}\beta)$. This line permits to derive the C^{++} abundance, which is the dominant ionization stage of C for the typical conditions of EHRs. There are only a few C abundance determinations available for EHRs, most of them derived from UV CELs that can only be observed from space (Garnett et al. 1995, 1999; Kobulnicky & Skillman 1998), and more recently from RLs (Esteban et al. 2002; Peimbert 2003; Tsamis et al. 2003; Peimbert et al. 2005; López-Sánchez et al. 2007; Bresolin 2007). The C abundance determinations based on UV CELs are severely affected by uncertainties in the reddening correction. To further complicate the situation, the STIS spectrograph aboard the *Hubble Space Telescope*, the only instrument capable to detect the UV CELs of C in bright EHRs, stopped science operations in 2004, so that nowadays the observation of the optical CII RLs provides the only possibility for determining C abundances in EHRs. The study of the behavior of C/H and C/O ratios and their galactocentric gradients in galaxies of different morphological types and metallicities is of paramount importance and can provide observational constraints for a better knowledge of the nucleosynthetic origin of carbon –the most important biogenic element– as well as the star formation/enrichment timescales in galaxies (e.g. Carigi et al. 2005).

O^{++} is the only ion that simultaneously shows bright CELs and detectable –relatively bright– RLs in the optical range. In H II regions, the O^{++} abundances derived from RLs are always between 0.10 and 0.35 dex higher than those derived from CELs (see compilation by García-Rojas & Esteban 2007). This observational fact is currently known as the “abundance discrepancy” (hereafter AD) problem. We define the abundance discrepancy factor (hereafter ADF) as the logarithmic difference between the abundance derived from RLs and CELs:

$$\text{ADF}(\text{X}^{i+}) = \log(\text{X}^{i+}/\text{H}^+)_{\text{RLs}} - \log(\text{X}^{i+}/\text{H}^+)_{\text{CELs}}, \quad (1)$$

where X^{i+} corresponds to the ionization state i of element X. Although the ADF found in H II regions is remarkably constant, this is not the case for planetary nebulae, PNe, where the values of the ADF can be quite different from object to object, with the ADFs ranging from near zero up to ten in some extreme cases (e.g. Liu 2006). This different behaviour

led García-Rojas & Esteban (2007) to the conclusion that the mechanism that produces the AD –or the bulk of it– in the extreme PNe should be different to that producing the AD in H II regions. The fact that the determination of nebular abundances is still uncertain, by at least a factor of two, has an important impact on many astrophysical aspects, such as chemical evolution and nucleosynthesis models and predictions, as well as the calibration of the so-called “strong line methods” used to estimate abundances in local and high-redshift star-forming galaxies. This last point was recently highlighted by Peimbert et al. (2007).

The origin of the AD problem is still object of debate and a challenge for our understanding of ionized nebulae. The results for a sample of Galactic H II regions seem to be consistent with the predictions of the temperature fluctuations paradigm (García-Rojas & Esteban 2007). In fact, in the presence of temperature fluctuations (parameterized by the mean square of the spatial variations of temperature, the t^2 parameter) the AD can be naturally explained because of the different temperature dependence of the intensity of RLs and CELs. However, the presence of temperature fluctuations in ionized nebulae still lacks a direct demonstration. An alternative explanation for the origin of the AD has been proposed by Tsamis & Péquignot (2005) and Stasińska et al. (2007), which is based on the presence of cold high-metallicity clumps of supernova ejecta still not mixed with the ambient gas of the H II regions. This cold gas would produce most of the emission of the RLs whereas the ambient gas of normal abundances would emit most of the intensity of CELs. However, López-Sánchez et al. (2007), who detect C II and O II lines in the dwarf galaxy NGC 5253, question this hypothesis in the light of the results available for EHRs.

Our group is interested in exploring the physical process that control the AD as well as in determining C abundances and radial gradients. In this paper, we make use of deep high-resolution spectrophotometry of a sample of bright EHRs in spiral and irregular galaxies as well as some giant H II regions in dwarf galaxies –H II galaxies– in order to explore a wide range of metallicities, H II regions of different sizes and structure, and galaxy morphological types. We think that this kind of study is necessary, mainly because the only intermediate-resolution spectral study devoted for the detection of RLs in EHRs of spiral galaxies was that by Esteban et al. (2002), which only included –apart from NGC 2363 in the irregular galaxy NGC 2366– three objects in two spirals (one in M 33 and two in M 101).

A highlight of this work is the use of high-spectral resolution spectrophotometry. These data are needed to increase the contrast between the faint RLs and the continuum, to deblend the O II lines of multiplet 1, and to separate them properly from possible Wolf-Rayet emission features as well as absorption features due to underlying stellar populations.

In §§ 2 and 3 of this paper we describe the observations, the data reduction procedure, the measurement of the emission lines, and the derivation of the reddening coefficient. In

§ 4 we derive the physical conditions of the nebulae and explore the consistency of different temperature scales, as well as calculate the ionic abundances from both kinds of lines: CELs and RLs. In § 5 we discuss the ADF in the sample objects and the radial C, O, and C/O abundance gradients in the spiral galaxies M 33, M 101, and NGC 2403. Finally, in § 6 we summarize our main conclusions.

2. Observations and Data Reduction

The observations of the sample objects, except NGC 5447 –a bright H II region in the galaxy M 101– were made on 2006 April 20 and 21 and November 14 with the High Resolution Echelle Spectrometer (HIRES, Vogt et al. 1994) at the Keck I telescope on Mauna Kea Observatory. The spectra cover the 3550–7440 Å range with a somewhat discontinuous wavelength coverage due to gaps between the detectors and to the fact that the redmost spectral orders do not fit completely within the CCD. The decker D3 was used, covering an area of $7''.0 \times 1''.7$. This configuration provides a spectral resolution of $R=23,000$. We observed a single slit position for each object. The center and position angle of the slits were chosen to cover the maximum area of the brightest part of the objects and the final usable one-dimensional spectra were extracted from an area of $5''.76 \times 1''.7$ for all the objects. The journal of the observations is shown in Table 1. The table includes the coordinates of the centers of the slits. In the case of the H II regions belonging to spiral galaxies with two or more objects observed –M33, NGC 2403, and M101, all of morphological type Sc– we also include the galactocentric distance (in kpc) and R/R_0 ratio of each H II region. The adopted distances to the galaxies have been taken from Freedman et al. (2001), and are 0.84, 3.22, and 7.5 Mpc for M33, NGC 2403, and M101, respectively. For M33, we have considered the photometric radius, R_0 , of $28'$ estimated by de Vaucouleurs et al. (1976), an inclination angle of 56° , and a position angle of 23° (Zaritsky et al. 1989). In the case of NGC 2403, we have adopted $R_0 = 8'.5$ (Zaritsky et al. 1994), $i = 60^\circ$, and $PA = 126^\circ$ (Garnett et al. 1997). Finally, for M101 we have assumed $R_0 = 14'.4$ (de Vaucouleurs et al. 1991), $i = 18^\circ$, and $PA = 37^\circ$ (Kamphuis 1993).

Intermediate-resolution spectroscopy of NGC 5447 was obtained on 2008 May 11 with the ISIS spectrograph at the 4.2m William Herschel Telescope (WHT) of the Observatorio del Roque de los Muchachos (La Palma, Spain). Two different CCDs were used at the blue and red arms of the spectrograph: an EEV CCD with a configuration 4100×2048 pixels with a pixel size of $13.5 \mu\text{m}$ in the blue arm and a REDPLUS CCD with 4096×2048 pixels with a pixel size of $15 \mu\text{m}$ in the red arm. The dichroic prism used to separate the blue and red beams was set at 5300 \AA . The slit was $3'.7$ long and $1''.03$ wide. Two gratings were used,

the R1200B in the blue arm and the R316R in the red arm. These gratings give reciprocal dispersions of 17 and 62 Å mm⁻¹, and effective spectral resolutions of 0.86 and 3.56 Å for the blue and red arms, respectively. The blue spectra cover from $\lambda\lambda 4225$ to 5075 Å and the red ones from $\lambda\lambda 5430$ to 8195 Å. The one-dimensional spectra were extracted from an area of $3''.2 \times 1''.03$, corresponding to the brightest zone of NGC 5447.

Standard data reduction procedures, including bias correction, flat-fielding, order extraction, wavelength calibrations, and flux calibration, were carried out using routines in the ECHELLE and ONEDSPEC packages of IRAF². The correction for atmospheric extinction was performed using the average curve for continuous atmospheric extinction at Mauna Kea and Roque de los Muchachos. The absolute flux calibration was achieved by observations of the standard stars Feige 34, Feige 66, Feige 110, H600, BD+25 4655, and BD+28 4211 in the case of the observations taken with the Keck I telescope and Feige 34, BD+25 3941, and BD+33 2624 in the case of the observations taken with the WHT.

3. Line intensities and Reddening Correction

Line intensities were measured integrating all the flux in the line between two given limits and over a local continuum estimated by eye. In the cases of line blending, a multiple Gaussian profile fit procedure was applied to obtain the line flux of each individual line. The measurements were performed with the SPLOT routine of the IRAF package.

Table 2 and Table 3 show the emission-line intensities measured for 10 EHRs where the RLs of O II and/or C II have been detected. Table 4 includes the emission-line intensities for 4 objects where those RLs were not detected. Due to their relevance to this paper, upper limits of the intensities of C II $\lambda 4267$ and/or O II $\lambda 4649$ –one of the brightest lines of multiple 1 of O II– at 1 σ level have been estimated and included in the tables for the objects where those RLs were not detected. For M 83, we cannot estimate appropriate upper limits of the intensities of C II and O II lines due to the contamination of spectral features produced by the underlying stellar emission to the continuum at low intensities. The first column of tables 2 to 4 includes the adopted laboratory wavelength, λ_0 , of the line. The second and third columns include the ion and identification of the line. The fourth column lists the reddening curve used (Seaton 1979). The following columns include –one pair of columns for each object– the observed wavelength in the heliocentric rest frame, λ , and the reddening-corrected flux relative to H β , $I(\lambda)$, of the lines. The identification and adopted laboratory wavelength of

²IRAF is distributed by National Optical Astronomical Observatories, operated by the Associated Universities for Research in Astronomy, Inc., under contract to the National Science Foundation

Table 1. Journal of observations

Host Galaxy	Object	R.A. ^a (J2000.0)	Decl. ^a (J2000.0)	R_G (kpc)	R/R_0	Date of Observation	Telescope	P.A. (deg)	Exposure Time (s)
M31	K932 ^b	00 46 34.0	+42 11 51	14/11/2006	Keck	330	3×1800
M33	NGC 595	01 33 34.2	+30 41 38	2.87	0.42	14/11/2006	Keck	90	3×1800
M33	NGC 604	01 34 33.3	+30 46 47	4.11	0.60	14/11/2006	Keck	90	3×1200
NGC 1741	Zone C ^c	05 01 37.6	-04 15 30	14/11/2006	Keck	50	2×1200
NGC 2366	NGC 2363	07 28 42.7	+69 11 26	20/04/2006	Keck	220	3×1800
NGC 2403	VS 24 ^d	07 36 45.7	+65 36 55	1.00	0.126	14/11/2006	Keck	295	3×1500
NGC 2403	VS 38 ^d	07 36 51.8	+65 36 42	1.04	0.131	14/11/2006	Keck	275	3×1650
NGC 2403	VS 44 ^d	07 37 06.8	+65 36 41	2.77	0.346	14/11/2006	Keck	330	3×1500
NGC 4395	Region #70 ^e	12 25 57.7	+33 31 32	21/04/2006	Keck	330	3×1800
NGC 4861	Brightest HII region ^f	12 59 00.1	+34 50 37	20/04/2006	Keck	220	3×1800
M83	Nucleus	13 36 59.8	-29 52 07	21/04/2006	Keck	90	3×1800
M101	H1013 ^g	14 03 32.2	+54 21 10	5.50	0.19	20/04/2006	Keck	270	4×1800
M101	NGC 5461	14 03 41.0	+54 19 01	9.84	0.34	20/04/2006	Keck	225	3×1800
M101	NGC 5447	14 02 28.7	+54 16 25	16.21	0.56	11/05/2008	WHT	134	7×1800

^aCoordinates of the slit center. Units of right ascension are hours, minutes, and seconds, and units of declination are degrees, arcminutes, and arcseconds.

^bWalterbos & Braun (1992) and Galarza et al. (1999)

^cHickson (1982)

^dVéron & Sauvayre (1965)

^eCedr s & Cepa (2002)

^fGil de Paz et al. (2003)

^gHodge et al. (1990)

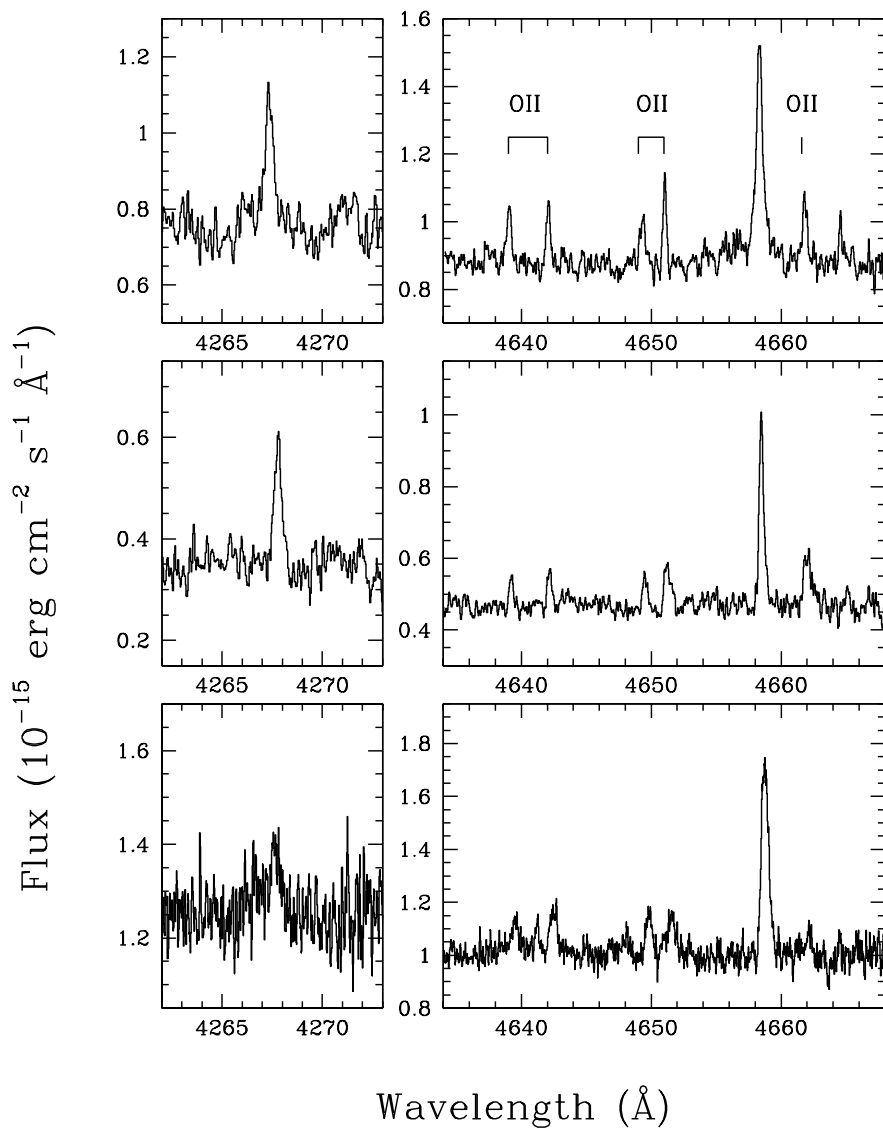


Fig. 1.— Sections of the spectra of NGC 604 (upper panels), K932 (middle panels), and NGC 2363 (lower panels) showing the C II λ 4267 (left) recombination line and the lines of multiplet 1 of O II $\sim\lambda\lambda$ 4650 (right).

the lines, as well as the error analysis applied, were obtained following García-Rojas et al. (2004), adding quadratically the error due to flux calibration that has been estimated to be 1 and 3 per cent for the November and April 2006 Keck I observations, respectively, and 4 per cent for the WHT observations. This flux calibration error corresponds to the standard deviation obtained from the calibration curves of the standard stars observed in each run. Colons indicate line flux errors of the order or greater than 40%.

A number of lines between 38 (M83-Nucleus) and 135 (NGC 2363) have been measured in the spectra of the 14 objects included in this study. A substantial fraction of them are permitted lines of heavy-element ions: C II, N I, O I, O II, and Si II; of these, only C II λ 4267 and the lines of multiplet 1 of O II at $\sim\lambda\lambda$ 4650 are pure RLs and can be used for abundance determinations. The rest of the permitted lines are mainly produced by fluorescence mechanisms (see Esteban et al. 2004). Only a small fraction of the lines are dubious identifications or could not be identified. Figure 1 contains sections of the spectra of three of the sample objects –NGC 604, K932 and NGC 2363– showing the C II λ 4267 line and the lines of multiplet 1 of O II.

All the sample objects have optical spectra published in the literature. In the case of the H II region K932 in M 31, only the intensities of a few bright emission lines have been reported (Galarza et al. 1999), no electron temperatures nor direct determinations of the chemical abundances were available for this object. This is the first time that C II and O II lines are detected in this object and in an H II region of M 31. The two H II regions observed in M 33, NGC 595 and NGC 604, were previously studied by Vílchez et al. (1988). Esteban et al. (2002) detected the C II and O II lines for the first time in NGC 604. There are no previous detections of those RLs in NGC 595. The nucleus –zone C– of the starburst galaxy NGC 1741 has been studied by López-Sánchez et al. (2004). These authors reported a dubious detection of a relatively bright emission feature tentatively identified as C II λ 4267 that has not been confirmed in our spectra. The giant H II region NGC 2363 in the irregular galaxy NGC 2366 has very detailed previous spectroscopical studies, such as those by González-Delgado et al. (1994) and Esteban et al. (2002). These last authors detected C II and O II lines for the first time in NGC 2363. The three H II regions observed in NGC 2403, VS 24, VS 38, and VS 44, were studied by Garnett et al. (1997). There are no previous detections of C II and O II lines for these objects. Region #70 of the spiral galaxy NGC 4395 had only very scarce spectral data available (McCall et al. 1985; Cedrés & Cepa 2002) and no electron temperature determinations. Optical spectra of the brightest region of the H II galaxy NGC 4861 were analyzed by Dinerstein & Shields (1986). A very deep spectrum of the center of M 83 has been obtained by Bresolin et al. (2005), who determine electron temperatures from more emission line ratios than in this study. It has been surprising not detecting C II and O II lines in our HIRES spectrum of the central H II

region of M 83 considering the high surface brightness and high metallicity of the nebula. However, this is a very low ionization degree object, its stellar underlying continuum is very high, and –most importantly– its emission lines are extremely broad. We consider that the high-spectral resolution used in our observation oversample too much the line profiles, producing a dramatical decrease of the intensity contrast of the fainter lines with respect to the strong continuum that prevents their detection. Finally, the three H II regions of M 101 observed in this paper, have also been studied in several works. H 1013 has been analyzed in depth by Bresolin (2007), who was the first in detecting C II lines in this object. NGC 5461 has been extensively studied in the literature (Rayo et al. 1982; Kennicutt & Garnett 1996; Esteban et al. 2002). Esteban et al. (2002) detected C II and O II lines in this object for the first time. Optical spectra of NGC 5447 have been analysed by Torres-Peimbert et al. (1989) and Kennicutt & Garnett (1996), but they do not determine electron temperatures, while Kennicutt et al. (2003) did so in three sub-components (H128, H143, H149) of this extended giant H II region. The line intensities reported in this paper do not show systematic differences with respect to those published in previous papers. They are consistent considering the expected differences due to aperture effects and/or extinction coefficients and reddening laws used.

It is interesting to note the identification of some lines of Ca I] at $\lambda\lambda$ 7394.08, 7423.6, 7442.99, 7457.3, and Ca I λ 7451.87 in the spectra of some of the sample objects. In particular, Ca I λ 7451.87 and Ca I] λ 7457.3 are rather bright, with dereddened intensities of the order of 1-3 % of $I(\text{H}\beta)$, and have been observed in 11 out of 13 objects for which we have spectra covering the spectral range redwards 7400 Å. We have carefully verified that all these lines do not correspond to sky emission features and that the wavelength calibration is accurate in that part of the spectrum. Therefore, they are real emission lines produced in the H II regions. It is striking that Ca I] and Ca I lines have not been previously identified in other H II regions from high-resolution echelle spectra published by our group (e.g. García-Rojas 2006; López-Sánchez et al. 2007). Moreover, we have not found references about their identification in other Galactic or extragalactic H II regions in the literature. The only exception is the detection of about 11 Ca I] lines in the spectral range between 7890 and 9700 Å in an unpublished VLT echelle spectrum that we obtained of a bright zone of the bar of the Orion Nebula. All the Ca I] lines detected in this paper are intercombination lines between the spectra terms $^3\text{F}^0$ and ^1D , and the single Ca I line detected corresponds to a $^3\text{F}^0$ – ^3D transition. Consistently, all the Ca I] lines detected in the bar of the Orion Nebula are also intercombination ones but, in this case, half of them correspond to a $^3\text{P}^0$ – ^1D transition. To find an explanation for the presence of these lines in the spectra is outside the scope of the present paper. However, the fact that similar lines have only been detected in the bar of the Orion Nebula and not in other similar spectra

–taken with the same instrument and with the same exposure time– of the central parts of the nebula (see Esteban et al. 2004), suggests that the Ca I] emission should be produced in the ionization edge of the EHRs observed in this paper, perhaps due to a fluorescence process at the photodissociation region (PDR). It would be interesting to further investigate the possible mechanism originating these transitions.

The observed line intensities of our objects must be corrected for interstellar reddening. This can be done using the reddening constant, $c(\text{H}\beta)$, obtained from the intensities of the Balmer lines. However, the fluxes of H I lines may be also affected by underlying stellar absorption. Consequently, we have performed an iterative procedure to derive both $c(\text{H}\beta)$ and the equivalent widths of the absorption in the hydrogen lines, W_{abs} , which we use to correct the observed line intensities. We assumed that the equivalent width of the absorption components is the same for all the Balmer lines and used the relation given by Mazzarella & Boroson (1993) for the absorption correction of each Balmer line following the procedure outlined by López-Sánchez et al. (2006). We have used the reddening curve of Seaton (1979) and the observed $\text{H}\alpha/\text{H}\beta$, $\text{H}\gamma/\text{H}\beta$, $\text{H}\delta/\text{H}\beta$, and $\text{H}\epsilon/\text{H}\beta$ line ratios. We have considered the theoretical line ratios expected for case B recombination given by Storey & Hummer (1995) for electron densities of 100 cm^{-3} and a first estimation of the electron temperature of each object based on the de-reddened line intensity ratios. In tables 2–4, we include the $c(\text{H}\beta)$ and W_{abs} pairs that provide the best match between the corrected and the theoretical line ratios. This procedure was not applied to NGC 5447 due to the fact that the shorter wavelength range covered in this object only includes three Balmer lines. Therefore, we have assumed that $W_{\text{abs}} = 0$ in the hydrogen lines for this object. In tables 2–4, we also include the observed (uncorrected for reddening) integrated $\text{H}\beta$ flux, $F(\text{H}\beta)$, the equivalent width of this line, $W(\text{H}\beta)$, and the equivalent width of the absorption in the hydrogen lines, W_{abs} .

The spectra of NGC 595, H 1013, and NGC 5461 show broad emission features centered at 4640 and 4686 Å. These two features –which are blended when observed at low spectral resolution but not in the present observations– correspond to the so-called Wolf-Rayet, W–R, blue bump originating from the stellar winds of these evolved massive stars. The brightest feature corresponds to He II $\lambda 4686$, and the emission at 4640 Å is the blend of N III $\lambda 4634$ and N III $\lambda 4640$, which are characteristic of W–R stars of the WNL subtype (Smith et al. 1996). In the cases of NGC 595, H 1013, and NGC 5461, those emission features were previously reported by Conti & Massey (1981), Bresolin (2007), and Rayo et al. (1982), respectively. In the case of NGC 5447, only a broad He II $\lambda 4686$ emission has been detected in our spectra. As far as we know, this is the first time that the broad He II $\lambda 4686$ emission feature is observed in the object.

In principle, the ratio between the integrated fluxes of the W–R blue bump and $\text{H}\beta$

can be used to estimate the W–R/O number ratio of a given star-forming region, however, our slit positions only cover a fraction of the total extension of the region and that ratio can not be properly derived from our observations. In any case, the observed integrated fluxes (uncorrected for reddening) of the W–R bumps at $\lambda 4640$ and $\lambda 4686$ are also included in Table 2.

Table 2. Dereddened line intensity ratios with respect to $I(\text{H}\beta)=100$ of NGC 595, NGC 604, H 1013, NGC 5461, and NGC 5447.

λ_0 (Å)	Ion	ID	$f(\lambda)$	NGC 595		NGC 604		H 1013		NGC 5461		NGC 5447	
				λ (Å)	$I(\lambda)$	λ (Å)	$I(\lambda)$	λ (Å)	$I(\lambda)$	λ (Å)	$I(\lambda)$	λ (Å)	$I(\lambda)$
3587.28	He I	32	0.278	3584.90	0.17 ± 0.05	3590.18	0.4 ± 0.1
3613.64	He I	6	0.275	3611.19	0.26 ± 0.05	3610.58	0.22 ± 0.05	3616.79	0.33 ± 0.09
3634.25	He I	28	0.272	3631.75	0.35 ± 0.05	3631.20	0.24 ± 0.06	3637.90	0.29 ± 0.08	3637.50	0.21 ± 0.08
3663.4	H I	H29	0.267	3660.35	0.21 ± 0.05
3664.68	H I	H28	0.267	3661.56	0.25 ± 0.06
3666.1	H I	H27	0.267	3663.63	0.19 ± 0.05	3662.97	0.26 ± 0.06
3667.68	H I	H26	0.266	3665.22	0.25 ± 0.05	3664.54	0.23 ± 0.05	3671.26	0.17:	3670.89	0.10:
3669.47	H I	H25	0.266	3667.00	0.29 ± 0.05	3666.40	0.21 ± 0.05	3673.05	0.28 ± 0.08	3672.64	0.13:
3671.48	H I	H24	0.266	3669.02	0.31 ± 0.05	3668.41	0.35 ± 0.06	3675.09	0.30 ± 0.08	3674.76	0.24 ± 0.09
3673.76	H I	H23	0.265	3671.27	0.28 ± 0.05	3670.69	0.38 ± 0.06	3677.40	0.30 ± 0.08	3676.92	0.33 ± 0.09
3676.37	H I	H22	0.265	3673.88	0.34 ± 0.05	3673.24	0.36 ± 0.06	3680.00	0.46 ± 0.09	3679.50	0.5 ± 0.1
3679.36	H I	H21	0.265	3676.87	0.43 ± 0.05	3676.23	0.42 ± 0.06	3682.96	0.40 ± 0.09	3682.51	0.5 ± 0.1
3682.81	H I	H20	0.264	3680.32	0.48 ± 0.06	3679.69	0.39 ± 0.06	3686.48	0.49 ± 0.09	3686.00	0.5 ± 0.1
3686.83	H I	H19	0.263	3684.35	0.55 ± 0.06	3683.75	0.54 ± 0.07	3690.52	0.6 ± 0.1	3690.01	0.6 ± 0.1
3691.56	H I	H18	0.263	3689.07	0.67 ± 0.06	3688.43	0.60 ± 0.07	3695.25	0.7 ± 0.1	3694.76	0.6 ± 0.1
3697.15	H I	H17	0.262	3694.65	0.76 ± 0.06	3694.03	0.68 ± 0.07	3700.83	0.8 ± 0.1	3700.32	0.8 ± 0.1
3703.86	H I	H16	0.260	3701.35	0.89 ± 0.06	3700.72	0.79 ± 0.07	3707.50	0.9 ± 0.1	3707.07	0.9 ± 0.1
3705.04	He I	25	0.260	3702.52	0.38 ± 0.05	3701.91	0.42 ± 0.06	3708.68	0.39 ± 0.09	3708.29	0.4 ± 0.1
3711.97	H I	H15	0.259	3709.47	1.08 ± 0.07	3708.83	0.88 ± 0.07	3715.65	1.1 ± 0.1	3715.19	1.0 ± 0.1
3721.83	[S III]	2F	0.257	3719.35	1.96 ± 0.08	3718.73	1.71 ± 0.09	3725.57	1.7 ± 0.1	3725.10	1.7 ± 0.2
3721.94	H I	H14
3726.03	[O II]	1F	0.257	3723.56	85 ± 1	3722.90	47.7 ± 0.9	3729.75	57 ± 2	3729.31	48 ± 2
3728.82	[O II]	1F	0.256	3726.31	120 ± 2	3725.65	67 ± 1	3732.51	78 ± 3	3732.03	55 ± 2
3734.37	H I	H13	0.255	3731.85	1.55 ± 0.07	3731.21	1.40 ± 0.08	3738.08	1.5 ± 0.1	3737.61	1.4 ± 0.1
3750.15	H I	H12	0.253	3747.62	1.78 ± 0.08	3746.98	1.97 ± 0.09	3753.89	2.0 ± 0.2	3753.41	1.9 ± 0.2
3770.63	H I	H11	0.249	3768.09	2.43 ± 0.09	3767.45	2.3 ± 0.1	3774.37	3.1 ± 0.2	3773.90	2.8 ± 0.2
3784.89	He I	64	0.246	3781.68	0.07:
3797.9	H I	H10	0.244	3795.34	3.3 ± 0.1	3794.69	3.1 ± 0.1	3801.67	4.2 ± 0.2	3801.18	4.2 ± 0.2
3819.61	He I	22	0.240	3817.03	0.73 ± 0.06	3816.39	0.92 ± 0.07	3823.41	0.8 ± 0.1	3822.93	0.8 ± 0.1
3835.39	H I	H9	0.237	3832.79	5.9 ± 0.1	3832.15	6.2 ± 0.1	3839.21	6.4 ± 0.3	3838.72	6.3 ± 0.3
3856.02	Si II	1	0.233	3859.30	0.12:
3862.59	Si II	1	0.232	3866.35	0.16:	3866.07	0.12:
3868.75	[Ne III]	1F	0.230	3866.09	1.54 ± 0.07	3865.51	8.0 ± 0.2	3872.67	2.8 ± 0.2	3872.14	15.2 ± 0.7

Table 2—Continued

λ_0 (Å)	Ion	ID	$f(\lambda)$	NGC 595		NGC 604		H 1013		NGC 5461		NGC 5447	
				λ (Å)	$I(\lambda)$	λ (Å)	$I(\lambda)$	λ (Å)	$I(\lambda)$	λ (Å)	$I(\lambda)$	λ (Å)	$I(\lambda)$
3871.82	He I	60	0.230
3889.05	H I	H8	0.226	3886.25	16.2 ± 0.3	3885.59	16.9 ± 0.3	3892.74	16.9 ± 0.7	3892.24	16.1 ± 0.7
3926.53	He I	58	0.219
3964.73	He I	5	0.211	3962.04	0.64 ± 0.05	3961.41	0.72 ± 0.06	3968.72	0.7 ± 0.1	3968.16	0.7 ± 0.1
3967.46	[Ne III]	1F	0.211	3964.73	0.44 ± 0.05	3964.13	2.49 ± 0.09	3971.43	0.8 ± 0.1	3970.90	4.7 ± 0.2
3970.07	H I	H7	0.210	3967.39	13.1 ± 0.2	3966.73	13.4 ± 0.2	3974.03	15.8 ± 0.6	3973.50	15.5 ± 0.7
4009.22	He I	55	0.202	4005.85	0.15 ± 0.04	4013.12	0.18 ± 0.07	4012.78	0.16:
4023.98	He I	54	0.198	4020.96	0.15 ± 0.04
4026.21	He I	18	0.198	4023.47	1.59 ± 0.07	4022.83	1.99 ± 0.08	4030.21	1.7 ± 0.1	4029.68	1.7 ± 0.1
4068.6	[S II]	1F	0.189	4065.90	0.73 ± 0.05	4065.16	1.19 ± 0.07	4072.64	0.7 ± 0.1	4072.20	0.9 ± 0.1
4076.35	[S II]	1F	0.187	4073.65	0.26 ± 0.04	4072.91	0.38 ± 0.05	4080.48	0.36 ± 0.08	4079.95	0.30 ± 0.08
4101.74	H I	H δ	0.182	4098.96	24.3 ± 0.4	4098.28	26.5 ± 0.4	4105.83	25.3 ± 0.9	4105.29	24 ± 1
4120.82	He I	16	0.177	4118.02	0.11 ± 0.04	4117.35	0.11 ± 0.04	4124.88	0.16:	4124.52	0.16:
4143.76	He I	53	0.172	4140.93	0.21 ± 0.04	4140.27	0.27 ± 0.05	4147.90	0.24 ± 0.07	4147.37	0.25 ± 0.07
4267.15	C II	6	0.144	4264.25	0.13 ± 0.03	4263.57	0.17 ± 0.04	4271.47	0.28 ± 0.08	4270.76	0.14:	4269.81	0.12 ± 0.03
4287.4	[Fe II]	7F	0.139	4283.73	0.08:	4291.20	0.14:
4303.82	O II	67	0.135	4300.29	0.07:	4308.37	0.13:
4317.14	O II	2	0.132	4313.54	0.10 ± 0.04
4340.47	H I	H γ	0.127	4337.52	45.0 ± 0.6	4336.81	47.9 ± 0.6	4344.78	44 ± 1	4344.21	44 ± 2	4343.02	48 ± 2
4363.21	[O III]	2F	0.121	4360.23	0.19 ± 0.04	4359.54	0.63 ± 0.05	4367.62	0.19 ± 0.07	4366.99	1.1 ± 0.1	4365.80	2.0 ± 0.1
4387.93	He I	51	0.115	4384.94	0.37 ± 0.04	4384.24	0.51 ± 0.05	4392.29	0.52 ± 0.09	4391.71	0.41 ± 0.08	4390.55	0.41 ± 0.05
4416.27	[Fe II]	6F	0.109	4420.31	0.08:
4437.55	He I	50	0.104	4433.86	0.08:	4439.87	0.11 ± 0.04
4471.09	He I	14	0.096	4468.46	3.56 ± 0.08	4467.74	4.31 ± 0.09	4474.14	4.2 ± 0.2
4634.14	N III	2	0.056	4638.36	0.03:
4638.86	O II	1	0.055	4634.92	0.07 ± 0.01	4642.79	0.04:	4641.80	0.07 ± 0.02
4640.64	N III	2	0.054	4644.73	0.03:
4641.81	O II	1	0.054	4637.95	0.05 ± 0.01	4645.73	0.04:	4644.50 ^a	0.12 ± 0.03
4649.13	O II	1	0.052	4645.89	0.05 ± 0.01	4645.22	0.05 ± 0.01	4653.62	0.07 ± 0.03	4653.23	0.08 ± 0.02	4653.00 ^b	0.13 ± 0.03
4650.84	O II	1	0.052	4647.67	0.05 ± 0.01	4646.95	0.08 ± 0.01	4655.49	0.06:	4655.10	0.05 ± 0.02
4658.1	[Fe III]	3F	0.050	4654.97	0.16 ± 0.01	4654.20	0.32 ± 0.02	4662.63	0.25 ± 0.04	4662.02	0.57 ± 0.04	4660.47	0.69 ± 0.07
4661.63	O II	1	0.049	4657.72	0.06 ± 0.01	4666.01	0.06:	4665.37	0.05:	4664.58	0.09 ± 0.02
4685.71	He II		0.043	4688.86	0.08 ± 0.02

Table 2—Continued

λ_0 (Å)	Ion	ID	$f(\lambda)$	NGC 595		NGC 604		H 1013		NGC 5461		NGC 5447	
				λ (Å)	$I(\lambda)$	λ (Å)	$I(\lambda)$	λ (Å)	$I(\lambda)$	λ (Å)	$I(\lambda)$	λ (Å)	$I(\lambda)$
4701.53	[Fe III]	3F	0.039	4697.61	0.11 ± 0.02	4706.26	0.14 ± 0.03	4705.51	0.21 ± 0.03	4704.27	0.19 ± 0.05
4711.37	[Ar IV]	1F	0.037	4714.22	0.19 ± 0.03
4713.14	He I	12	0.036	4709.96	0.29 ± 0.02	4709.20	0.38 ± 0.02	4717.89	0.30 ± 0.04	4717.24	0.39 ± 0.03	4716.02	0.36 ± 0.03
4733.93	[Fe III]	3F	0.031	4738.16	0.6:	4737.92	0.07 ± 0.02
4740.16	[Ar IV]	1F	0.030	4743.86	0.10 ± 0.02	4743.06	0.15 ± 0.02
4754.83	[Fe III]	3F	0.026	4750.82	0.05 ± 0.01	4758.93	0.15 ± 0.02	4757.48	0.08:
4769.6	[Fe III]	3F	0.023	4773.63	0.06 ± 0.02
4861.33	H I	H β	0.000	4858.04	100 ± 1	4857.24	100 ± 1	4866.16	100 ± 3	4865.52	100 ± 3	4864.22	100 ± 4
4881	[Fe III]	2F	-0.005	4876.96	0.09 ± 0.01	4885.21	0.17 ± 0.02	4883.58	0.16 ± 0.03
4921.93	He I	48	-0.015	4918.60	0.88 ± 0.02	4917.81	1.04 ± 0.03	4926.83	1.05 ± 0.06	4926.19	1.04 ± 0.05	4924.90	1.01 ± 0.03
4924.5	[Fe III]	2F	-0.016	4928.85	0.11 ± 0.02
4931.32	[O III]	1F	-0.017	4935.25	0.09 ± 0.02	4934.36	0.05:
4958.91	[O III]	1F	-0.024	4955.53	28.7 ± 0.3	4954.77	68.4 ± 0.7	4963.90	33 ± 1	4963.26	103 ± 3	4961.93	135 ± 5
4985.9	[Fe III]	2F	-0.031	4982.48	0.21 ± 0.01	4981.64	0.43 ± 0.02	4990.82	0.32 ± 0.04	4990.00	0.38 ± 0.03	4988.77	0.40 ± 0.04
5006.84	[O III]	1F	-0.036	5003.43	92 ± 1	5002.67	211 ± 2	5011.88	97 ± 3	5011.23	302 ± 9	5009.88	410 ± 17
5015.68	He I	4	-0.038	5012.27	1.87 ± 0.03	5011.46	2.02 ± 0.04	5020.69	1.99 ± 0.09	5020.03	2.00 ± 0.08	5018.68	2.0 ± 0.1
5041.03	Si II	5	-0.044	5037.55	0.08 ± 0.01	5036.82	0.12 ± 0.01	5046.03	0.14 ± 0.03	5045.45	0.17 ± 0.02
5047.74	He I	47	-0.046	5044.30	0.11 ± 0.01	5043.48	0.16 ± 0.02	5052.70	0.13 ± 0.03	5052.13	0.13 ± 0.02
5055.98	Si II	5	-0.048	5052.60	0.08 ± 0.01	5051.87	0.07 ± 0.01	5061.11	0.11 ± 0.03	5060.46	0.16 ± 0.02
5158.81	[Fe II]	19F	-0.073	5163.35	0.05 ± 0.02
5197.9	[N I]	1F	-0.082	5194.53	0.11 ± 0.01	5193.56	0.25 ± 0.02	5203.12	0.33 ± 0.04	5202.53	0.31 ± 0.03
5200.26	[N I]	1F	-0.083	5196.88	0.10 ± 0.01	5195.87	0.20 ± 0.02	5205.49	0.26 ± 0.04	5204.78	0.21 ± 0.03
5261.61	[Fe II]	19F	-0.098	5266.43	0.04:
5270.4	[Fe III]	1F	-0.100	5266.97	0.08 ± 0.01	5266.11	0.18 ± 0.02	5275.89	0.18 ± 0.04	5275.07	0.28 ± 0.03
5317.8	O II	...	-0.111	5322.36	0.03:
5517.71	[Cl III]	1F	-0.154	5513.96	0.42 ± 0.02	5513.07	0.36 ± 0.02	5523.20	0.39 ± 0.05	5522.50	0.44 ± 0.04	5521.40	0.56 ± 0.07
5537.88	[Cl III]	1F	-0.158	5534.11	0.33 ± 0.02	5533.19	0.27 ± 0.02	5543.36	0.25 ± 0.04	5542.63	0.31 ± 0.03	5541.76	0.41 ± 0.04
5676.02	N II	3	-0.181	5681.60	0.02:
5679.56	N II	3	-0.182	5685.19	0.05:
5754.64	[N II]	3F	-0.194	5750.76	0.39 ± 0.02	5749.77	0.27 ± 0.02	5760.33	0.43 ± 0.05	5759.60	0.34 ± 0.03	5758.52	0.29 ± 0.03
5875.64	He I	11	-0.215	5871.68	10.2 ± 0.2	5870.74	10.7 ± 0.2	5881.54	11.3 ± 0.5	5880.77	11.6 ± 0.6	5879.63	12.5 ± 0.7
5957.56	Si II	4	-0.228	5963.92	0.07 ± 0.03	5963.16	0.07 ± 0.02
5978.93	Si II	4	-0.231	5973.93	0.07 ± 0.01	5984.89	0.09 ± 0.03	5984.19	0.06 ± 0.02

Table 2—Continued

λ_0 (Å)	Ion	ID	$f(\lambda)$	NGC 595		NGC 604		H 1013		NGC 5461		NGC 5447	
				λ (Å)	$I(\lambda)$	λ (Å)	$I(\lambda)$	λ (Å)	$I(\lambda)$	λ (Å)	$I(\lambda)$	λ (Å)	$I(\lambda)$
6046.23	O I	22	-0.242	6041.24 ^c	0.02:
6046.44													
6046.49													
6300.3	[O I]	1F	-0.282	6296.20	0.67 ± 0.02	6295.02	1.14 ± 0.04	6306.81	1.44 ± 0.09	6305.82	1.11 ± 0.07	6304.96	2.3 ± 0.2
6312.1	[S III]	3F	-0.283	6318.38	0.72 ± 0.06	6317.59	1.16 ± 0.08	6316.38	1.2 ± 0.1
6347.11	Si II	2	-0.289	6342.81	0.064 ± 0.008	6341.78	0.07 ± 0.01	6353.38	0.13 ± 0.03	6352.62	0.14 ± 0.02
6363.78	[O I]	1F	-0.291	6359.62	0.23 ± 0.01	6358.42	0.39 ± 0.02	6370.16	0.31 ± 0.04	6369.34	0.39 ± 0.03	6368.28	0.53 ± 0.07
6371.36	Si II	2	-0.292	6367.06	0.055 ± 0.008	6366.02	0.07 ± 0.01	6377.73	0.14 ± 0.03	6376.92	0.10 ± 0.02
	?		-0.311	6508.26	0.07 ± 0.03
6500.83	O II		-0.311	6506.60	0.02:
6548.03	[N II]	1F	-0.318	6543.71	13.1 ± 0.4	6554.59	20 ± 1	6553.76	10.0 ± 0.7	6552.53	6.1 ± 0.5
6562.82	H I	H α	-0.320	6558.38	299 ± 9	6557.31	275 ± 9	6569.34	282 ± 16	6568.49	277 ± 19	6567.26	297 ± 19
6578.05	C II	2	-0.322	6573.61	0.18 ± 0.01	6572.55	0.12 ± 0.01	6584.58	0.23 ± 0.04	6583.67	0.11 ± 0.02
6583.41	[N II]	1F	-0.323	6579.07	45.6 ± 1.4	6577.92	26.5 ± 0.9	6590.02	59 ± 3	6589.16	29 ± 2	6587.81	17 ± 1
6678.15	He I	46	-0.336	6673.63	2.9 ± 0.1	6672.56	2.9 ± 0.1	6684.83	3.1 ± 0.2	6683.96	3.2 ± 0.2	6682.70	3.2 ± 0.2
6716.47	[S II]	2F	-0.342	6712.03	12.7 ± 0.4	6710.83	14.8 ± 0.5	6723.16	14.9 ± 0.9	6722.26	11.5 ± 0.8	6721.07	10.0 ± 0.7
6730.85	[S II]	2F	-0.344	6726.39	9.0 ± 0.3	6725.19	10.6 ± 0.4	6737.56	11.0 ± 0.7	6736.69	9.7 ± 0.7	6735.47	8.2 ± 0.6
7001.92	O I	21	-0.379	6996.24	0.028 ± 0.007	7008.45	0.03:
7065.28	He I	10	-0.387	7072.35	1.7 ± 0.1	7071.48	2.6 ± 0.2	7070.04	2.2 ± 0.2
	?		-0.390	7082.59	0.10 ± 0.03
7135.78	[Ar III]	1F	-0.396	7130.95	6.9 ± 0.3	7129.81	7.1 ± 0.3	7142.93	6.8 ± 0.5	7142.02	8.8 ± 0.8	7140.60	9.4 ± 0.7
7231.34	C II	3	-0.408	7226.42	0.063 ± 0.008	7225.26	0.06 ± 0.01
7236.42	C II	3	-0.409	7231.51	0.10 ± 0.01	7230.43	0.10 ± 0.01
7281.35	He I	45	-0.414	7275.32	0.28 ± 0.02	7288.70	0.40 ± 0.05	7287.65	0.45 ± 0.05
7318.39	[O II]	2F	-0.418	7314.19	0.48 ± 0.03	7312.96	0.36 ± 0.03	7327.25 ^d	1.1 ± 0.1	7326.33 ^d	1.6 ± 0.2	7325.07 ^d	1.8 ± 0.2
7319.99	[O II]	2F	-0.418	7315.24	1.07 ± 0.05	7314.00	0.90 ± 0.05
7329.66	[O II]	2F	-0.420	7324.79	0.67 ± 0.03	7323.56	0.56 ± 0.04	7334.81 ^e	1.5 ± 0.1
7330.73	[O II]	2F	-0.420	7325.88	0.63 ± 0.03	7324.64	0.50 ± 0.03
7377.83	[Ni II]	2F	-0.425	7384.05	0.15 ± 0.03	7384.30	0.04 ± 0.01
7423.6	Ca I]		-0.431	7417.64	0.040 ± 0.009	7431.22	0.05 ± 0.02
7442.99	Ca I]		-0.433	7438.82	0.040 ± 0.007	7450.93	0.07 ± 0.02	7449.75	0.07 ± 0.02
7451.87	Ca I]		-0.434	7447.12	2.3 ± 0.1	7445.82	1.55 ± 0.09	7459.52	1.8 ± 0.1	7458.57	1.2 ± 0.1
7457.3	Ca I]		-0.434	7452.62	3.2 ± 0.2	7451.32	2.5 ± 0.1	7465.05	2.2 ± 0.2	7464.03	1.2 ± 0.1

Table 2—Continued

λ_0 (Å)	Ion	ID	$f(\lambda)$	NGC 595		NGC 604		H 1013		NGC 5461		NGC 5447	
				λ (Å)	$I(\lambda)$	λ (Å)	$I(\lambda)$	λ (Å)	$I(\lambda)$	λ (Å)	$I(\lambda)$	λ (Å)	$I(\lambda)$
7468.31	N I	3	-0.436	7463.55	0.059 ± 0.008	7476.10	0.08 ± 0.02	7474.99	0.06 ± 0.02
c(H β)					0.39 ± 0.02		0.47 ± 0.02		0.22 ± 0.04		0.42 ± 0.04		0.48 ± 0.07
F(H β) (10^{-13} erg cm $^{-2}$ s $^{-1}$)					2.4 ± 0.1		4.2 ± 0.2		1.5 ± 0.1		8.1 ± 0.8		1.5 ± 0.3
–W(H β) (Å)					77		179		119		160		136
W _{abs} (Å)					1.8		0.0		0.0		0.5		...
F(W–Rb λ 4640) (10^{-15} erg cm $^{-2}$ s $^{-1}$)					4.0 ± 0.1		...		1.83 ± 0.08		2.1 ± 0.2		...
F(W–Rb λ 4686) (10^{-15} erg cm $^{-2}$ s $^{-1}$)					8.4 ± 0.2		...		2.73 ± 0.08		4.2 ± 0.2		1.06 ± 0.08

^aBlended with the W–R blue bump emission at 4640 Å.

^bBlend of O II λ 4649.13 and λ 4650.84 lines.

^cBlend of O I λ 6046.23, λ 6046.44, and λ 6046.49 lines.

^dBlend of [O II] λ 7318.39 and λ 7319.99 lines.

^eBlend of [O II] λ 7329.66 and λ 7330.73 lines.

Table 3. Dereddened line intensity ratios with respect to $I(\text{H}\beta)=100$ of VS 24, VS 38, VS 44, NGC 2363, and K932

λ_0 (Å)	Ion	ID	$f(\lambda)$	VS 24		VS 38		VS 44		NGC 2363		K 932	
				λ (Å)	$I(\lambda)$	λ (Å)	$I(\lambda)$	λ (Å)	$I(\lambda)$	λ (Å)	$I(\lambda)$	λ (Å)	$I(\lambda)$
3554.42	He I	34	0.283	3555.37	0.22 ± 0.03
3587.28	He I	32	0.278	3589.02	0.22 ± 0.06	3588.20	0.17 ± 0.03	3586.52	0.34 ± 0.08
3613.64	He I	6	0.275	3614.41	0.3 ± 0.1	3615.24	0.23 ± 0.06	3614.55	0.22 ± 0.03	3612.91	0.46 ± 0.09
3634.25	He I	28	0.272	3634.96	0.3 ± 0.1	3635.86	0.12:	3635.19	0.29 ± 0.03	3633.51	0.49 ± 0.09
3661.22	H I	H31	0.267	3662.20	0.05:	3660.49	0.27 ± 0.08
3662.26	H I	H30	0.267	3662.99	0.2:	3663.18	0.07 ± 0.02	3661.54	0.23 ± 0.08
3663.4	H I	H29	0.267	3664.19	0.2:	3664.30	0.12 ± 0.03	3662.67	0.34 ± 0.08
3664.68	H I	H28	0.267	3665.47	0.20: 0.09	3665.62	0.15 ± 0.03	3663.84	0.21 ± 0.08
3666.1	H I	H27	0.267	3666.88	0.3 ± 0.1	3667.03	0.19 ± 0.03	3665.35	0.31 ± 0.08
3667.68	H I	H26	0.266	3668.39	0.3 ± 0.1	3668.62	0.23 ± 0.03	3666.91	0.36 ± 0.08
3669.47	H I	H25	0.266	3670.20	0.3 ± 0.1	3670.41	0.26 ± 0.03	3668.74	0.37 ± 0.08
3671.48	H I	H24	0.266	3672.22	0.4 ± 0.1	3673.19	0.27 ± 0.06	3672.41	0.29 ± 0.03	3670.72	0.45 ± 0.09
3673.76	H I	H23	0.265	3674.50	0.4 ± 0.1	3675.40	0.28 ± 0.06	3674.70	0.32 ± 0.03	3672.99	0.51 ± 0.09
3676.37	H I	H22	0.265	3677.12	0.4 ± 0.1	3677.93	0.33 ± 0.07	3677.31	0.39 ± 0.03	3675.62	0.63 ± 0.09
3679.36	H I	H21	0.265	3680.12	0.4 ± 0.1	3680.95	0.52 ± 0.07	3680.28	0.40 ± 0.03	3678.60	0.69 ± 0.09
3682.81	H I	H20	0.264	3683.56	0.6 ± 0.1	3684.48	0.62 ± 0.08	3683.73	0.49 ± 0.04	3682.08	0.73 ± 0.09
3686.83	H I	H19	0.263	3687.59	0.7 ± 0.1	3688.49	0.77 ± 0.08	3687.79	0.56 ± 0.04	3686.09	0.86 ± 0.09
3691.56	H I	H18	0.263	3692.32	0.8 ± 0.1	3692.60	0.41 ± 0.08	3693.18	0.47 ± 0.07	3692.50	0.64 ± 0.04	3690.81	0.93 ± 0.09
3697.15	H I	H17	0.262	3697.90	0.8 ± 0.1	3698.28	0.52 ± 0.09	3698.71	0.66 ± 0.08	3698.10	0.80 ± 0.05	3696.40	1.11 ± 0.09
3703.86	H I	H16	0.260	3704.61	0.9 ± 0.1	3704.94	0.60 ± 0.09	3705.46	0.70 ± 0.08	3704.78	0.85 ± 0.05	3703.11	1.4 ± 0.1
3705.04	He I	25	0.260	3705.76	0.3 ± 0.1	3706.55	0.28 ± 0.06	3705.96	0.42 ± 0.03	3704.25	0.66 ± 0.09
3711.97	H I	H15	0.259	3712.73	1.1 ± 0.1	3713.08	0.9 ± 0.1	3713.57	0.73 ± 0.08	3712.92	1.08 ± 0.06	3711.21	1.5 ± 0.1
3721.83	[S III]	2F	0.257	3722.65	1.7 ± 0.1	3723.04	1.5 ± 0.1	3723.50	1.6 ± 0.1	3722.81	1.94 ± 0.09	3721.09	2.7 ± 0.1
3721.94	H I	H14											
3726.03	[O II]	1F	0.257	3726.83	65 ± 1	3727.14	45.7 ± 0.8	3727.66	58 ± 1	3726.99	11.4 ± 0.5	3725.27	65 ± 1
3728.82	[O II]	1F	0.256	3729.57	78 ± 1	3729.90	61 ± 1	3730.42	75 ± 1	3729.76	13.8 ± 0.6	3728.02	78 ± 1
3734.37	H I	H13	0.255	3735.12	1.6 ± 0.1	3735.49	1.5 ± 0.1	3736.02	1.21 ± 0.09	3735.32	1.58 ± 0.07	3733.61	2.3 ± 0.1
3750.15	H I	H12	0.253	3750.91	2.1 ± 0.1	3751.29	2.0 ± 0.1	3751.78	1.5 ± 0.1	3751.12	2.2 ± 0.1	3749.38	3.0 ± 0.1
3770.63	H I	H11	0.249	3771.39	2.7 ± 0.1	3771.76	2.3 ± 0.1	3772.29	2.2 ± 0.1	3771.60	3.0 ± 0.1	3769.86	3.9 ± 0.1
3797.9	H I	H10	0.244	3798.66	3.6 ± 0.1	3799.04	3.0 ± 0.1	3799.56	2.7 ± 0.1	3798.88	4.5 ± 0.2	3797.12	5.1 ± 0.1
3805.74	He I	58	0.242	3806.73	0.07 ± 0.02
3819.61	He I	22	0.240	3820.38	0.6 ± 0.1	3820.74	0.7 ± 0.1	3821.34	0.57 ± 0.07	3820.60	0.82 ± 0.05	3818.85	1.08 ± 0.09
3835.39	H I	H9	0.237	3836.16	6.0 ± 0.2	3836.54	6.0 ± 0.2	3837.11	5.4 ± 0.2	3836.38	6.4 ± 0.3	3834.61	7.3 ± 0.2

Table 3—Continued

λ_0 (Å)	Ion	ID	$f(\lambda)$	VS 24		VS 38		VS 44		NGC 2363		K 932	
				λ (Å)	$I(\lambda)$	λ (Å)	$I(\lambda)$	λ (Å)	$I(\lambda)$	λ (Å)	$I(\lambda)$	λ (Å)	$I(\lambda)$
3856.02	Si II	1	0.233	3857.72	0.25 ± 0.06
3862.59	Si II	1	0.232	3864.14	0.19 ± 0.05	3863.61	0.04:
3867.49	He I	20	0.231	3868.38	0.05:
3868.75	[Ne III]	1F	0.230	3869.56	5.5 ± 0.2	3869.93	5.3 ± 0.2	3870.53	6.8 ± 0.2	3869.75	47 ± 2	3867.98	15.8 ± 0.3
3871.82	He I	60	0.230	3872.80	0.07 ± 0.02
3889.05	H I	H8	0.226	3889.65	15.8 ± 0.3	3890.02	18.0 ± 0.3	3890.62	15.2 ± 0.3	3889.85	18.1 ± 0.7	3888.09	19.4 ± 0.3
3926.53	He I	58	0.219	3927.59	0.10 ± 0.02
3964.73	He I	5	0.211	3965.54	0.41 ± 0.09	3965.92	0.48 ± 0.08	3966.52	0.58 ± 0.07	3965.76	0.67 ± 0.04	3963.93	0.86 ± 0.08
3967.46	[Ne III]	1F	0.211	3968.36	1.0 ± 0.1	3968.67	1.6 ± 0.1	3969.25	2.1 ± 0.1	3968.49	13.9 ± 0.5	3966.66	4.9 ± 0.1
3970.07	H I	H7	0.210	3970.88	12.7 ± 0.2	3971.28	13.1 ± 0.3	3971.86	12.6 ± 0.3	3971.09	15.3 ± 0.6	3969.27	15.9 ± 0.3
4009.22	He I	55	0.202	4011.13	0.13 ± 0.05	4010.27	0.15 ± 0.03	4008.45	0.16:
4026.21	He I	18	0.198	4027.01	1.5 ± 0.1	4027.42	1.7 ± 0.1	4028.03	1.6 ± 0.1	4027.23	1.70 ± 0.07	4025.39	1.94 ± 0.09
4068.6	[S II]	1F	0.189	4069.43	0.9 ± 0.1	4069.79	0.66 ± 0.09	4070.40	1.16 ± 0.08	4069.65	0.40 ± 0.03	4067.77	0.72 ± 0.08
4069.62	O II	10	0.189	4070.98	0.06 ± 0.02	4068.90	0.18 ± 0.07
4069.89	O II	10
4076.35	[S II]	1F	0.187	4077.20	0.27 ± 0.09	4078.15	0.39 ± 0.06	4077.39	0.13 ± 0.01	4075.56	0.32 ± 0.07
4101.74	H I	H δ	0.182	4102.54	24.9 ± 0.4	4102.96	26.7 ± 0.4	4103.58	25.1 ± 0.4	4102.79	25.4 ± 0.9	4100.90	26.4 ± 0.4
4120.82	He I	16	0.177	4122.93	0.13 ± 0.05	4121.89	0.18 ± 0.01	4120.11	0.21 ± 0.07
4143.76	He I	53	0.172	4145.61	0.19 ± 0.05	4144.83	0.26 ± 0.01	4142.92	0.25 ± 0.07
4168.97	He I	52	0.167	4170.09	0.056 ± 0.008	4168.25	0.14:
4227.91	[Ni III]?		0.153	4228.58	0.038 ± 0.008
4267.15	C II	6	0.144	4268.11	0.15:	4268.29	0.20 ± 0.06	4269.12	0.10 ± 0.04	4268.38	0.035 ± 0.007	4266.35	0.22 ± 0.06
4287.4	[Fe II]	7F	0.139	4288.15	0.27 ± 0.08	4289.26	0.08:	4288.45	0.027 ± 0.007
4340.47	H I	H γ	0.127	4341.31	46.1 ± 0.6	4341.76	47.2 ± 0.6	4342.42	45.9 ± 0.6	4341.57	44 ± 1	4339.58	47.1 ± 0.6
4359.34	[Fe II]	7F	0.122	4361.29	0.12 ± 0.04	4360.41	0.028 ± 0.007
4363.21	[O III]	2F	0.121	4364.16	0.43 ± 0.08	4364.49	0.60 ± 0.08	4365.15	0.62 ± 0.06	4364.28	13.7 ± 0.5	4362.31	0.95 ± 0.07
4368.19	O I	5	0.120	4370.13	0.10:
4368.25	O I	5
4387.93	He I	51	0.115	4388.81	0.29 ± 0.08	4389.23	0.31 ± 0.07	4389.90	0.38 ± 0.06	4389.04	0.43 ± 0.02	4387.03	0.54 ± 0.06
4413.78	[Fe II]	7F	0.109	4415.74	0.08:
4437.55	He I	50	0.104	4436.39	0.13:
4471.09	He I	14	0.096	4472.37	3.4 ± 0.1	4472.84	3.9 ± 0.1	4473.53	3.9 ± 0.1	4470.59	4.34 ± 0.09
4621.39	N II	5	0.059	4622.99	0.013:

Table 3—Continued

λ_0 (Å)	Ion	ID	$f(\lambda)$	VS 24		VS 38		VS 44		NGC 2363		K 932	
				λ (Å)	$I(\lambda)$	λ (Å)	$I(\lambda)$	λ (Å)	$I(\lambda)$	λ (Å)	$I(\lambda)$	λ (Å)	$I(\lambda)$
4638.86	O II	1	0.055	4641.10	0.04 ± 0.02	4640.01	0.018 ± 0.006	4637.94	0.06 ± 0.01
4640.64	N III	2	0.054	4642.66	0.07 ± 0.02
4641.81	O II	1	0.054	4643.98	0.04 ± 0.02	4642.98	0.027 ± 0.007	4640.86	0.06 ± 0.01
4649.13	O II	1	0.052	...	<0.07	...	<0.07	4653.13	0.06 ± 0.02	4650.27	0.021 ± 0.006	4648.18	0.06 ± 0.01
4650.84	O II	1	0.052	4655.53	0.06 ± 0.02	4651.91	0.036 ± 0.007	4649.95	0.12 ± 0.02
4658.1	[Fe III]	3F	0.050	4659.10	0.34 ± 0.04	4659.53	0.21 ± 0.04	4660.15	0.59 ± 0.03	4659.29	0.12 ± 0.01	4657.17	0.33 ± 0.02
4661.63	O II	1	0.049	4663.70	0.10 ± 0.02	4662.87	0.024 ± 0.006	4660.70	0.07 ± 0.01
4685.71	He II		0.043	4687.10	0.25 ± 0.01
4701.53	[Fe III]	3F	0.039	4703.72	0.14 ± 0.02	4702.79	0.030 ± 0.007	4700.65	0.09 ± 0.01
4711.37	[Ar IV]	1F	0.037	4712.53	2.24 ± 0.07	4710.57	0.05 ± 0.01
4713.14	He I	12	0.036	4714.13	0.21 ± 0.03	4714.58	0.25 ± 0.04	4715.28	0.33 ± 0.03	4714.35	0.53 ± 0.02	4712.21	0.40 ± 0.02
4740.16	[Ar IV]	1F	0.030	4741.38	1.74 ± 0.06	4739.43	0.04 ± 0.01
4744.35	[Fe IV] ?		0.029	4743.33	0.03 ± 0.01
4754.83	[Fe III]	3F	0.026	4756.90	0.11 ± 0.02	4755.90	0.021 ± 0.006	4753.78	0.05 ± 0.01
4769.6	[Fe III]	3F	0.023	4768.51	0.05 ± 0.01
4861.33	H I	H β	0.000	4862.27	100 ± 1	4862.77	100 ± 1	4863.52	100 ± 1	4862.55	100 ± 3	4860.34	100 ± 1
4881	[Fe III]	2F	-0.005	4882.06	0.11 ± 0.03	4883.10	0.19 ± 0.02	4882.29	0.039 ± 0.007	4880.02	0.07 ± 0.01
4899.97	[Fe IV]		-0.009	4901.11	0.017 ± 0.006
4902.65	Si II	7.23	-0.010	4904.10	0.047 ± 0.007
4906.56	[Fe IV]		-0.011	4907.76	0.037 ± 0.007
4917.98	[Fe IV]		-0.014	4919.32	0.018 ± 0.007
4921.93	He I	48	-0.015	4922.89	0.82 ± 0.05	4923.38	0.76 ± 0.06	4924.17	0.96 ± 0.03	4923.19	1.00 ± 0.03	4920.94	1.11 ± 0.03
4931.32	[O III]	1F	-0.017	4932.46	0.082 ± 0.009
4958.91	[O III]	1F	-0.024	4959.93	48.1 ± 0.5	4960.40	50.2 ± 0.6	4961.20	64.4 ± 0.7	4960.17	234 ± 7	4957.92	93 ± 1
4979.87	N II		-0.029	4979.03	0.07 ± 0.01
4979.92	N II		
4985.9	[Fe III]	2F	-0.031	4986.80	0.33 ± 0.04	4987.33	0.30 ± 0.03	4988.07	0.64 ± 0.03	4987.12	0.11 ± 0.01	4984.81	0.19 ± 0.02
5006.84	[O III]	1F	-0.036	5007.88	145 ± 2	5008.35	151 ± 2	5009.16	193 ± 2	5008.12	572 ± 17	5005.84	283 ± 3
5015.68	He I	4	-0.038	5016.66	1.79 ± 0.06	5017.17	1.98 ± 0.08	5017.94	1.85 ± 0.04	5016.95	1.77 ± 0.06	5014.66	2.13 ± 0.04
5028.6	[Fe III]		-0.041	5029.84	0.051 ± 0.008
5031.34	[Cr III]?		-0.042	5032.48	0.027 ± 0.006
5033.59	[Fe IV]		-0.042	5034.98	0.022 ± 0.006
5036.56	[Fe II]		-0.043	5037.64	0.013:

Table 3—Continued

λ_0 (Å)	Ion	ID	$f(\lambda)$	VS 24		VS 38		VS 44		NGC 2363		K 932	
				λ (Å)	$I(\lambda)$	λ (Å)	$I(\lambda)$	λ (Å)	$I(\lambda)$	λ (Å)	$I(\lambda)$	λ (Å)	$I(\lambda)$
5041.03	Si II	5	-0.044	5042.15	0.14 ± 0.03	5043.26	0.14 ± 0.02	5042.39	0.054 ± 0.008	5039.99	0.11 ± 0.01
5047.74	He I	47	-0.046	5048.78	0.09 ± 0.03	5050.06	0.09 ± 0.02	5049.01	0.16 ± 0.01	5046.71	0.17 ± 0.02
5055.98	Si II	5	-0.048	5057.05	0.15 ± 0.03	5058.33	0.15 ± 0.02	5057.47	0.030 ± 0.007	5055.04	0.10 ± 0.01
5158.81	[Fe II]	19F	-0.073	5160.10	0.014 ± 0.006
5191.82	[Ar III]	3F	-0.081	5193.02	0.085 ± 0.009
5197.9	[N I]	1F	-0.082	5199.03	0.27 ± 0.03	5199.52	0.13 ± 0.03	5200.22	0.38 ± 0.03	5199.23	0.105 ± 0.009	5196.88	0.26 ± 0.02
5200.26	[N I]	1F	-0.083	5201.38	0.20 ± 0.03	5201.85	0.11 ± 0.03	5202.65	0.27 ± 0.02	5201.59	0.050 ± 0.008	5199.25	0.20 ± 0.02
5233.46	[Fe IV]		-0.091	5234.89	0.015 ± 0.006
5261.61	[Fe II]	19F	-0.098	5262.92	0.014 ± 0.006
5270.4	[Fe III]	1F	-0.100	5271.69	0.17 ± 0.03	5272.90	0.28 ± 0.02	5271.79	0.063 ± 0.008
5273.38	[Fe II]	18F	-0.100	5274.70	0.010:
5274.81	[Fe II]		-0.101	5275.97	0.014 ± 0.006
5322.99	[Cl IV]		-0.112	5324.41	0.018 ± 0.006
5412	[Fe III]	1F	-0.134	5413.24	0.028 ± 0.007
5512.77	O I	25	-0.153	5514.13	0.015 ± 0.006
5517.71	[Cl III]	1F	-0.154	5518.78	0.35 ± 0.04	5519.32	0.28 ± 0.04	5520.22	0.35 ± 0.03	5519.10	0.25 ± 0.01	5516.57	0.40 ± 0.02
5537.88	[Cl III]	1F	-0.158	5538.94	0.27 ± 0.04	5539.46	0.14 ± 0.03	5540.35	0.26 ± 0.02	5539.24	0.18 ± 0.01	5536.72	0.32 ± 0.02
5577.34	[O I]	3F	-0.164	5578.70	0.025 ± 0.006
5754.64	[N II]	3F	-0.194	5755.74	0.35 ± 0.04	5756.32	0.23 ± 0.04	5757.17	0.33 ± 0.03	5756.08	0.047 ± 0.008	5753.42	0.39 ± 0.02
5875.64	He I	11	-0.215	5876.81	10.0 ± 0.2	5877.44	11.2 ± 0.2	5878.33	10.5 ± 0.2	5877.14	10.3 ± 0.4	5874.48	11.7 ± 0.2
5957.56	Si II	4	-0.228	5960.59	0.08 ± 0.02	5959.48	0.027 ± 0.007
5978.93	Si II	4	-0.231	5981.60	0.09 ± 0.02	5980.43	0.025 ± 0.006	5977.71	0.06 ± 0.01
6300.3	[O I]	1F	-0.282	6301.62	0.88 ± 0.05	6302.24	0.38 ± 0.03	6303.12	1.39 ± 0.05	6301.90	0.93 ± 0.04	6299.07	0.66 ± 0.02
6312.1	[S III]	3F	-0.283	6313.35	0.86 ± 0.05	6313.95	0.55 ± 0.04	6314.96	0.96 ± 0.05	6313.66	1.24 ± 0.06	6310.80	1.11 ± 0.04
6347.11	Si II	2	-0.289	6349.96	0.11 ± 0.03	6345.79	0.075 ± 0.007
6363.78	[O I]	1F	-0.291	6365.13	0.30 ± 0.04	6365.76	0.17 ± 0.02	6366.59	0.48 ± 0.04	6365.40	0.32 ± 0.02	6362.51	0.23 ± 0.01
6371.36	Si II	2	-0.292	6372.55	0.11 ± 0.03	6374.17	0.09 ± 0.02	6372.96	0.034 ± 0.004	6370.09	0.075 ± 0.007
6548.03	[N II]	1F	-0.318	6549.36	13.1 ± 0.4	6550.01	9.4 ± 0.2	6550.99	10.5 ± 0.3	6549.72	0.58 ± 0.03	6546.74	10.4 ± 0.3
6562.82	H I	H α	-0.320	6564.09	280 ± 8	6564.76	275 ± 6	6565.78	281 ± 8	6564.44	257 ± 12	6561.48	293 ± 10
6578.05	C II	2	-0.322	6579.32	0.16 ± 0.04	6579.87	0.17 ± 0.02	6581.01	0.09 ± 0.02	6579.75	0.007 ± 0.002
6583.41	[N II]	1F	-0.323	6584.75	39 ± 1	6585.39	27.5 ± 0.7	6586.37	30.5 ± 0.8	6585.10	1.74 ± 0.09	6582.10	32 ± 1
6678.15	He I	46	-0.336	6679.46	2.7 ± 0.1	6680.15	2.85 ± 0.09	6681.20	2.9 ± 0.1	6679.82	2.6 ± 0.1	6676.82	3.2 ± 0.1
6716.47	[S II]	2F	-0.342	6717.79	14.2 ± 0.4	6718.46	10.7 ± 0.3	6719.43	16.4 ± 0.5	6718.17	3.8 ± 0.2	6715.11	8.9 ± 0.3

Table 3—Continued

λ_0 (Å)	Ion	ID	$f(\lambda)$	VS 24		VS 38		VS 44		NGC 2363		K 932	
				λ (Å)	$I(\lambda)$	λ (Å)	$I(\lambda)$	λ (Å)	$I(\lambda)$	λ (Å)	$I(\lambda)$	λ (Å)	$I(\lambda)$
6730.85	[S II]	2F	-0.344	6732.17	10.9 ± 0.3	6732.83	7.8 ± 0.2	6733.80	12.5 ± 0.4	6732.54	3.0 ± 0.2	6729.48	6.9 ± 0.3
6734	C II	21	-0.344	6735.83	0.062 ± 0.006
6739.8	[Fe IV]		-0.345	6741.57	0.034 ± 0.004
6761.3	[Fe IV]		-0.348	6762.97	0.013 ± 0.003
6795.1	[K IV]?		-0.352	6796.66	0.020 ± 0.004
7065.28	He I	10	-0.387	7066.71	1.57 ± 0.08	7067.34	1.16 ± 0.06	7068.47	1.81 ± 0.08
7080.57	[Cr III]?		-0.389	7082.08	0.022 ± 0.004
7135.78	[Ar III]	1F	-0.396	7137.20	5.8 ± 0.2	7137.90	5.9 ± 0.2	7139.03	6.7 ± 0.2	7137.57	4.4 ± 0.3	7134.33	8.7 ± 0.4
7170.5	[Ar IV]		-0.401	7172.38	0.074 ± 0.007
7281.35	He I	45	-0.414	7282.80	0.31 ± 0.04	7283.54	0.23 ± 0.03	7284.67	0.47 ± 0.04	7283.21	0.48 ± 0.03	7279.87	0.46 ± 0.03
7318.39	[O II]	2F	-0.418	7320.69	0.45 ± 0.05	7321.25	0.22 ± 0.03	7322.98	1.41 ± 0.07	7321.74 ^a	0.74 ± 0.05	7317.51	0.34 ± 0.02
7319.99	[O II]	2F	-0.418	7321.67	0.86 ± 0.06	7322.31	0.61 ± 0.04	7323.54	0.33 ± 0.03			7318.62	1.06 ± 0.06
7329.66	[O II]	2F	-0.420	7331.24	0.57 ± 0.05	7331.92	0.46 ± 0.04	7333.09	0.92 ± 0.05	7332.02 ^b	0.63 ± 0.04	7328.12	0.55 ± 0.03
7330.73	[O II]	2F	-0.420	7332.27	0.46 ± 0.05	7333.00	0.23 ± 0.03	7334.20	0.44 ± 0.04			7329.27	0.62 ± 0.04
7394.08	Ca I		-0.427	7396.17	0.016 ± 0.003
	?		-0.429	7409.68	0.022 ± 0.004
7423.6	Ca I		-0.431	7425.78	0.036 ± 0.005
7442.99	Ca I		-0.433	7445.41	0.073 ± 0.007
7451.87	Ca I		-0.434	7453.65	1.65 ± 0.09	7454.33	1.93 ± 0.08	7455.42	1.77 ± 0.09	7454.04	0.42 ± 0.03	7450.57	1.23 ± 0.07
7457.3	Ca I		-0.434	7459.11	2.0 ± 0.1	7459.82	2.4 ± 0.1	7460.91	1.78 ± 0.09	7459.54	0.50 ± 0.03	7456.09	1.41 ± 0.08
$c(H\beta)$				0.34 ± 0.02		0.20 ± 0.02		0.33 ± 0.02		0.12 ± 0.04		0.47 ± 0.02	
$F(H\beta)$ (10^{-13} erg cm $^{-2}$ s $^{-1}$)				2.2 ± 0.1		0.71 ± 0.03		3.0 ± 0.1		5.5 ± 0.5		2.4 ± 0.1	
$-W(H\beta)$ (Å)				29		33		130		363		149	
W_{abs} (Å)				0.3		0.0		1.3		0.0		0.0	

^aBlend of [O II] λ 7318.39 and λ 7319.99 lines.^bBlend of [O II] λ 7329.66 and λ 7330.73 lines.

Table 4. Dereddened line intensity ratios with respect to $I(\text{H}\beta)=100$ of NGC 1741-C, NGC 4395-70, NGC 4861, and M83-Nucleus.

λ_0 (Å)	Ion	ID	$f(\lambda)$	NGC 1741-C		NGC 4395-70		NGC 4861		M83-Nucleus	
				λ (Å)	$I(\lambda)$	λ (Å)	$I(\lambda)$	λ (Å)	$I(\lambda)$	λ (Å)	$I(\lambda)$
3554.42	He I	34	0.283	3564.15	0.19 ± 0.05
3587.28	He I	32	0.278	3597.06	0.22 ± 0.05
3613.64	He I	6	0.275	3623.51	0.31 ± 0.06
3634.25	He I	28	0.272	3644.13	0.35 ± 0.06
3666.1	H I	H27	0.267	3675.99	0.18 ± 0.05
3667.68	H I	H26	0.266	3677.76	0.22 ± 0.05
3669.47	H I	H25	0.266	3679.47	0.26 ± 0.05
3671.48	H I	H24	0.266	3681.45	0.34 ± 0.06
3673.76	H I	H23	0.265	3683.77	0.41 ± 0.06
3676.37	H I	H22	0.265	3686.38	0.48 ± 0.06
3679.36	H I	H21	0.265	3689.38	0.63 ± 0.07
3682.81	H I	H20	0.264	3692.85	0.81 ± 0.07
3686.83	H I	H19	0.263	3696.88	0.85 ± 0.07
3691.56	H I	H18	0.263	3701.58	0.94 ± 0.08
3697.15	H I	H17	0.262	3746.14	0.9 ± 0.3	3707.23	1.06 ± 0.08	3703.09	0.8:
3703.86	H I	H16	0.260	3753.20	1.2 ± 0.3	3714.18	1.6 ± 0.1
3711.97	H I	H15	0.259	3761.23	1.4 ± 0.3	3722.09	1.50 ± 0.09	3718.17	0.7:
3721.83	[S III]	2F	0.257	3771.29	1.7 ± 0.3	3725.74	1.4 ± 0.5	3731.96	2.8 ± 0.1	3728.17	0.9 ± 0.3
3721.94	H I	H14									
3726.03	[O II]	1F	0.257	3775.56	58 ± 2	3729.96	44 ± 2	3736.18	37 ± 1	3732.36	18 ± 1
3728.82	[O II]	1F	0.256	3778.31	75 ± 3	3732.71	64 ± 3	3738.94	49 ± 2	3735.05	17 ± 1
3734.37	H I	H13	0.255	3783.95	1.4 ± 0.3	3744.52	2.0 ± 0.1	3740.56	1.1 ± 0.4
3750.15	H I	H12	0.253	3799.88	1.9 ± 0.3	3760.37	2.6 ± 0.1	3756.49	0.8:
3770.63	H I	H11	0.249	3820.59	2.7 ± 0.3	3774.63	2.5 ± 0.5	3780.91	3.7 ± 0.2	3776.94	2.1 ± 0.4
3797.9	H I	H10	0.244	3848.21	3.6 ± 0.4	3801.92	3.6 ± 0.5	3808.25	5.0 ± 0.2	3804.27	2.6 ± 0.5
3819.61	He I	22	0.240	3830.03	0.82 ± 0.07
3835.39	H I	H9	0.237	3886.19	6.1 ± 0.4	3839.50	5.2 ± 0.5	3845.83	7.0 ± 0.3	3841.84	4.4 ± 0.6
3856.02	Si II	1	0.233	3862.25	0.5:
3862.59	Si II	1	0.232	3866.80	0.8:
3868.75	[Ne III]	1F	0.230	3920.02	18.6 ± 0.8	3872.88	21 ± 1	3879.32	45 ± 2	3875.73	1.2 ± 0.4
3871.82	He I	60	0.230	3876.73	2.6 ± 0.5
3889.05	H I	H8	0.226	3940.40	15.5 ± 0.7	3892.97	14.4 ± 0.8	3899.46	18.9 ± 0.7	3895.49	10.9 ± 0.9
3964.73	He I	5	0.211	3975.51	0.79 ± 0.07

Table 4—Continued

λ_0 (Å)	Ion	ID	$f(\lambda)$	NGC 1741-C		NGC 4395-70		NGC 4861		M83-Nucleus	
				λ (Å)	$I(\lambda)$	λ (Å)	$I(\lambda)$	λ (Å)	$I(\lambda)$	λ (Å)	$I(\lambda)$
3967.46	[Ne III]	1F	0.211	4020.07	5.3 ± 0.4	3971.64	8.7 ± 0.6	3978.28	14.9 ± 0.6
3970.07	H I	H7	0.210	4022.69	13.7 ± 0.6	3974.28	15.6 ± 0.8	3980.89	16.7 ± 0.6	3976.80	13.3 ± 0.9
4009.22	He I	55	0.202	4019.99	0.20 ± 0.05
4026.21	He I	18	0.198	4079.83	1.4 ± 0.3	4030.42	1.3 ± 0.4	4037.17	1.7 ± 0.1
4068.6	[S II]	1F	0.189	4122.64	1.5 ± 0.3	4072.87	2.2 ± 0.5	4079.72	1.00 ± 0.08	4075.65	1.0 ± 0.3
4076.35	[S II]	1F	0.187	4080.98	1.6 ± 0.4	4087.42	0.38 ± 0.06
4101.74	H I	H6	0.182	4156.09	24.5 ± 0.9	4106.09	24 ± 1	4112.92	26.9 ± 0.9	4108.67	22 ± 1
4120.82	He I	16	0.177	4131.98	0.15 ± 0.05
4143.76	He I	53	0.172	4154.98	0.22 ± 0.05
4267.15	C II	6	0.144	...	<0.1	...	<0.1	...	<0.03
4287.4	[Fe II]	7F	0.139	4344.53	0.6 ± 0.2	4299.10	0.10:
4340.47	H I	H γ	0.127	4397.98	46 ± 2	4345.06	42 ± 1	4352.29	46 ± 1	4347.80	42 ± 2
4359.34	[Fe II]	7F	0.122	4371.27	0.07:
4363.21	[O III]	2F	0.121	4421.00	1.1 ± 0.3	4367.80	2.5 ± 0.4	4375.10	8.2 ± 0.3
4387.93	He I	51	0.115	4399.85	0.38 ± 0.06
4413.78	[Fe II]	7F	0.109	4425.88	0.10:
4649.13	O II	1	0.052	...	<0.1	...	<0.1	...	<0.04
4658.1	[Fe III]	3F	0.050	4720.21	0.9 ± 0.1	4670.82	0.59 ± 0.05
4685.71	He II		0.043	4698.56	0.66 ± 0.05
4701.53	[Fe III]	3F	0.039	4763.77	0.35 ± 0.09	4714.38	0.21 ± 0.04
4711.37	[Ar IV]	1F	0.037	4724.27	0.88 ± 0.06
4713.14	He I	12	0.036	4725.93	0.49 ± 0.05
4740.16	[Ar IV]	1F	0.030	4753.18	0.69 ± 0.05
4754.83	[Fe III]	3F	0.026	4767.59	0.13 ± 0.03
4769.6	[Fe III]	3F	0.023	4782.52	0.10 ± 0.03
4861.33	H I	H β	0.000	4925.75	100 ± 3	4866.48	100 ± 3	4874.57	100 ± 3	4869.48	100 ± 3
4881	[Fe III]	2F	-0.005	4894.28	0.16 ± 0.03
4921.93	He I	48	-0.015	4987.21	0.7 ± 0.1	4927.26	0.7 ± 0.1	4935.35	0.99 ± 0.06
4958.91	[O III]	1F	-0.024	5024.62	103 ± 3	4964.15	109 ± 3	4972.45	208 ± 6	4967.57	2.4 ± 0.2
4985.9	[Fe III]	2F	-0.031	5052.27	1.0 ± 0.1	4991.21	1.2 ± 0.2	4999.46	0.69 ± 0.05
5006.84	[O III]	1F	-0.036	5073.18	305 ± 9	5012.14	318 ± 10	5020.51	607 ± 18	5015.39	9.8 ± 0.4
5015.68	He I	4	-0.038	5082.16	1.5 ± 0.1	5021.02	1.7 ± 0.2	5029.34	1.92 ± 0.08	5024.35	0.9 ± 0.1
5041.03	Si II	5	-0.044	5054.84	0.11 ± 0.03

Table 4—Continued

λ_0 (Å)	Ion	ID	$f(\lambda)$	NGC 1741-C		NGC 4395-70		NGC 4861		M83-Nucleus	
				λ (Å)	$I(\lambda)$	λ (Å)	$I(\lambda)$	λ (Å)	$I(\lambda)$	λ (Å)	$I(\lambda)$
5047.74	He I	47	-0.046	5061.47	0.14 ± 0.03
5055.98	Si II	5	-0.048	5069.92	0.07:	5064.68	1.0 ± 0.1
5191.82	[Ar III]	3F	-0.081	5205.76	0.08 ± 0.03
5197.9	[N I]	1F	-0.082	5203.32	0.8 ± 0.1	5212.20	0.22 ± 0.04	5206.70	1.0 ± 0.1
5200.26	[N I]	1F	-0.083	5205.77	0.4 ± 0.1	5214.54	0.10 ± 0.03	5209.01	1.1 ± 0.1
5261.61	[Fe II]	19F	-0.098	5275.98	0.06:
5270.4	[Fe III]	1F	-0.100	5340.95	0.41 ± 0.09	5284.93	0.23 ± 0.04
5273.38	[Fe II]	18F	-0.100	5426.93	0.06:
5325.14	[Fe II]		-0.113	5330.76	0.3:
5455.25	[Fe II]		-0.144	5461.11	0.3:
5517.71	[Cl III]	1F	-0.154	5523.50	0.4 ± 0.1	5532.76	0.45 ± 0.04
5537.88	[Cl III]	1F	-0.158	5543.69	0.4 ± 0.1	5552.89	0.31 ± 0.04
5754.64	[N II]	3F	-0.194	5831.03	0.34 ± 0.09	5760.73	0.2:	5770.19	0.10 ± 0.03	5764.29	0.19 ± 0.07
5875.64	He I	11	-0.215	5953.51	11.0 ± 0.4	5881.89	9.5 ± 0.5	5891.69	10.9 ± 0.4	5885.63	6.2 ± 0.4
6300.3	[O I]	1F	-0.282	6383.92	2.8 ± 0.2	6307.16	6.3 ± 0.4	6317.55	1.70 ± 0.08
6312.1	[S III]	3F	-0.283	6395.82	1.09 ± 0.09	6318.83	1.4 ± 0.2	6329.32	2.04 ± 0.09	6322.90	0.18:
of the spectra 6347.11	Si II	2	-0.289	6357.90	0.4 ± 0.1
6363.78	[O I]	1F	-0.291	6448.08	0.80 ± 0.08	6370.56	1.1 ± 0.1	6381.20	0.55 ± 0.03	6374.52	0.24 ± 0.09
6371.36	Si II	2	-0.292	6388.83	0.08 ± 0.01	6382.20	0.28 ± 0.09
6548.03	[N II]	1F	-0.318	6634.82	7.8 ± 0.3	6555.08	4.6 ± 0.3	6565.92	1.52 ± 0.07	6559.13	50 ± 4
6562.82	H I	H α	-0.320	6649.80	286 ± 10	6569.77	261 ± 13	6580.68	284 ± 12	6573.84	300 ± 27
6583.41	[N II]	1F	-0.323	6670.70	26.1 ± 0.9	6590.49	14.2 ± 0.8	6601.39	4.4 ± 0.2	6594.56	147 ± 14
6678.15	He I	46	-0.336	6685.25	2.4 ± 0.2	6696.35	3.0 ± 0.1	6689.34	1.8 ± 0.2
6716.47	[S II]	2F	-0.342	6805.63	21.1 ± 0.8	6723.63	25 ± 1	6734.79	9.3 ± 0.4	6727.73	22 ± 2
6730.85	[S II]	2F	-0.344	6820.21	14.7 ± 0.6	6738.02	18 ± 1	6749.20	7.0 ± 0.3	6742.16	24 ± 2
7065.28	He I	10	-0.387	7158.91	1.7 ± 0.1	7072.75	1.4 ± 0.2	7084.50	2.3 ± 0.1	7077.19	1.1 ± 0.2
7075.24	[Fe II]		-0.389	7082.85	0.5 ± 0.1
7135.78	[Ar III]	1F	-0.396	7230.33	6.5 ± 0.3	7143.33	7.3 ± 0.5	7155.23	7.5 ± 0.4	7147.92	1.6 ± 0.3
7281.35	He I	45	-0.414	7378.02	0.29 ± 0.06	7301.18	0.47 ± 0.03
7318.39	[O II]	2F	-0.418	7416.97 ^a	1.3 ± 0.1	7327.73 ^a	1.8 ± 0.2
7329.66	[O II]	2F	-0.420	7427.47 ^b	1.3 ± 0.1
7377.83	[Ni II]	2F	-0.425	7398.27	0.032 ± 0.007
7423.6	Ca I]		-0.431	...	of the spectra	7444.58	0.08 ± 0.01

4. Physical Conditions and Chemical Abundances

4.1. Electron Temperatures and Densities

The physical conditions of the ionized gas: electron temperatures, T_e , and densities, n_e , have been derived from the usual CEL ratios, using the IRAF task `temden` of the package NEBULAR (Shaw & Dufour 1995) with updated atomic data for some ions (see García-Rojas et al. 2005, their table 4). Electron densities have been derived from [N I] $\lambda\lambda 5198/5200$, [O II] $\lambda\lambda 3726/3729$, [S II] $\lambda\lambda 6717/6731$, [Cl III] $\lambda\lambda 5518/5538$, and [Ar IV] $\lambda\lambda 4711/4740$ line ratios. Electron temperatures have been calculated using four sets of auroral to nebular line intensity ratios: [N II] $\lambda 5755$ /[N II] $\lambda\lambda 6548, 6583$, [O II] $\lambda\lambda 7319, 7330$ /[O II] $\lambda\lambda 3726, 3729$, [S II] $\lambda\lambda 4069, 4076$ /[S II] $\lambda\lambda 6717, 6731$, and [O III] $\lambda 4363$ /[O III] $\lambda\lambda 4959, 5007$. The procedure for the determination of the physical conditions was the following: an initial T_e -value of 10,000 K was assumed in order to derive a first approximation to the different n_e determinations; then these preliminary n_e -values were used to recompute T_e , and finally, we iterated until convergence to obtain the adopted values of n_e and T_e . T_e ([O II]) and T_e ([N II]) have been corrected from the contribution to [O II] $\lambda\lambda 7319, 7330$ and [N II] $\lambda 5755$, respectively, due to recombination following the formulae derived by Liu et al. (2000). These contributions are between 4 and 6% in the case of the intensity of [O II] $\lambda\lambda 7319, 7330$ lines and between 1 and 3% for the intensity of [N II] $\lambda 5755$. It is necessary to estimate the N^{++}/H^+ ratio for determining the recombination contribution to the intensity of the auroral line of [N II]. In all the cases, we have estimated this abundance ratio considering a preliminary determination of the N^+ , O^+ , and O^{++} abundances and assuming that O^{++}/O^+ is approximately N^{++}/N^+ . In the case of NGC 2363, its T_e ([O II]) is above the range of validity (5000 to 10,000 K) of the formula of Liu et al. (2000) for the correction due to recombination of the [O II] $\lambda\lambda 7319, 7330$ lines. Therefore, the correction we estimate for this object could not be correct. However, the fact that the recombination rate decreases with temperature implies that this effect should be very small in NGC 2363. The physical conditions determined for all the sample objects are shown in Table 5.

All the sample objects show low densities, with values lower than 10^3 cm^{-3} and even near the low density limit in some cases. The central H II region of M 83 shows the largest n_e , three different indicators giving consistent results of about 700 cm^{-3} . There are three objects where the n_e has been derived from the [Ar IV] line ratio, in all the cases this indicator gives larger densities than the other line ratios and about 10^3 cm^{-3} , suggesting some density stratification in these nebulae. In fact, Ar^{3+} is the ion with the highest ionization potential for which we can derive n_e , and its associated Strömgen sphere should be located in the innermost parts of the nebula.

Table 4—Continued

λ_0 (Å)	Ion	ID	$f(\lambda)$	NGC 1741-C		NGC 4395-70		NGC 4861		M83-Nucleus	
				λ (Å)	$I(\lambda)$	λ (Å)	$I(\lambda)$	λ (Å)	$I(\lambda)$	λ (Å)	$I(\lambda)$
7442.99	Ca I]		-0.433	7463.90	0.11 ± 0.01
7451.87	Ca I		-0.434	7460.06	2.2 ± 0.2	7472.35	1.24 ± 0.07
7457.3	Ca I]		-0.434	7465.55	3.0 ± 0.3	7477.91	1.29 ± 0.07
$c(\text{H}\beta)$				0.19 ± 0.02		0.17 ± 0.04		0.04 ± 0.04		0.52 ± 0.05	
$F(\text{H}\beta)$				1.23 ± 0.07		1.9 ± 0.2		2.6 ± 0.3		7.5 ± 0.9	
$-W(\text{H}\beta)$				73		28		137		27	
W_{abs}				1.1		0.0		0.0		0.4	

^aBlend of [O II] $\lambda 7318.39$ and $\lambda 7319.99$ lines.

^bBlend of [O II] $\lambda 7329.66$ and $\lambda 7330.73$ lines.

Table 5. Physical conditions

Parameter	Lines	NGC 595	NGC 604	H1013	NGC 5461	NGC 5447	VS 24	VS 38
N_e (cm ⁻³)	[N I]	270±180	140±100	114 ⁺¹⁴⁰ ₋₁₁₄	<100	...	<100	220 ⁺³²⁰ ₋₂₂₀
	[O II]	260±30	270±30	280±60	540±110	...	450±40	310±30
	[S II]	<100	<100	<100	260±160	220±170	120±50	<100
	[Cl III]	700±370	490 ⁺⁵¹⁰ ₋₄₉₀	70 ⁺⁷⁸⁰ ₋₇₀	180 ⁺⁴⁶⁰ ₋₁₈₀	280 ⁺⁶⁹⁰ ₋₂₈₀	640 ⁺⁹³⁰ ₋₆₄₀	50 ⁺¹⁸⁰⁰ ₋₅₀
	[Ar IV]	1170 ⁺²⁰²⁰ ₋₁₁₇₀
T_e (K)	[N II]	8400±160	8950±270	7970±370	9310±400	10950±610	8530±340	8260±470
	[O II]	7760±100	9190±160	6010±370	7810±160	7720±150
	[S II]	7070±260	8350±330	...	7280±500	...	6990±420	...
	[O III]	7450±330	8150±160	7370±630	8470±200	9280±180	8100±410	8730±330
		VS 44	NGC 2363	K932	NGC 1741-C	NGC 4395-70	NGC 4861	M 83-Nucleus
N_e (cm ⁻³)	[N I]	<100	<100	103±80	...	<100	<100	740±380
	[O II]	370±40	550±100	470±40	380±40	240±60	400±80	720±120
	[S II]	110±50	165±120	130±80	<100	<100	100±100	670±110
	[Cl III]	480 ⁺⁶¹⁰ ₋₄₈₀	20 ⁺⁴³⁰ ₋₂₀	740±480
	[Ar IV]	...	1150±550	1200±1100	...
T_e (K)	[N II]	9050±280	13800±1300	9500±200	9800±1100	10800±2800	12500±2200	5100±310
	[O II]	9500±180	15450±700	9300±150	8860±240
	[S II]	7450±290	9220±480	8350±560	...	9600±1400	8800±500	...
	[O III]	8270±210	16200±300	8360±150	8450±520	10700±600	12900±200	...

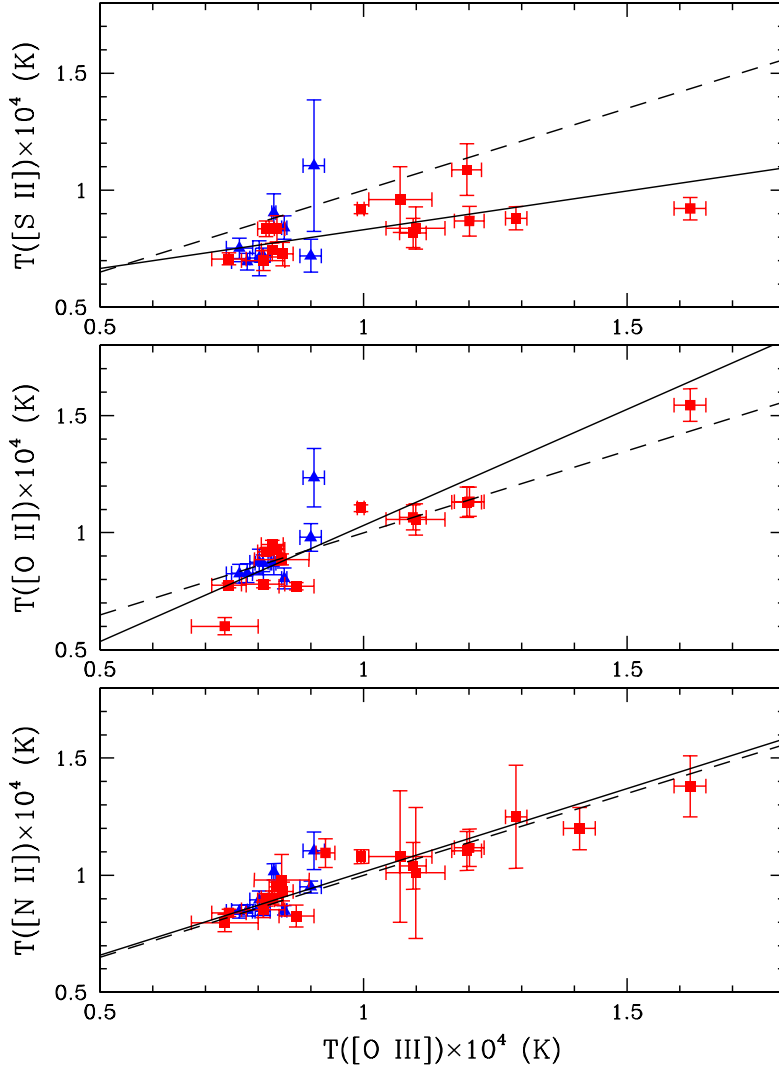


Fig. 2.— Correlations between various T_e diagnostics. Filled (red) squares show our measurements for extragalactic H II regions and those of NGC 5253 from López-Sánchez et al. (2007), 30 Doradus from Peimbert (2003), and NGC 5471 from Esteban et al. (2002). Filled (blue) triangles show measurements for a sample of Galactic H II regions taken from the compilation by García-Rojas & Esteban (2007). The solid lines represent the least-squares fit of the measurements. The dashed lines show the predicted correlations from Garnett (1992) based on photoionization models.

The data compiled in Table 5 provides a relatively large number of different T_e determinations, in particular those associated with low ionization potential ions: [N II], [O II], and [S II]. This allows us to compare the consistency of different temperature scales. Garnett (1992) constructed photoionization models that provide simple scaling relations between temperatures measured from different ions. This author obtains the following relation between T_e ([O III]) and other temperature indicators of low ionization degree ions –such as T_e ([N II]), T_e ([O II]), and T_e ([S II])– valid for the temperature range from 2000 to 18,000 K:

$$T_e(\text{[N II]}) = T_e(\text{[O II]}) = T_e(\text{[S II]}) = 0.70 \times T_e(\text{[O III]}) + 3000 \text{ K.} \quad (2)$$

Similar relationships between T_e ([O III]) and T_e ([O II]) have been obtained by other authors (Campbell et al. 1986; Izotov et al. 1994; Pilyugin et al. 2006) and have been extensively used in many works. Several authors have tried to make observational tests of the reliability of these relations (Garnett et al. 1997; Kennicutt et al. 2003; Pérez-Montero & Díaz 2003; Hägele et al. 2006, 2008; Bresolin et al. 2009). The T_e ([N II]) vs. T_e ([O III]) relationship has been the most difficult one to test because of the paucity of good determinations of the T_e ([N II]) temperature indicator. This is because most studies have focused on the determination of chemical abundances in low-metallicity, high-excitation EHRs, especially H II galaxies, where the [N II] λ 5755 line is very faint (Pérez-Montero & Díaz 2003; Hägele et al. 2006, 2008). Kennicutt et al. (2003) studied H II regions in M 101, a group of objects whose properties are more similar to those of most of our EHRs, but the small number of objects with T_e ([N II]) determinations in their sample does not permit to obtain a clear trend between T_e ([N II]) and T_e ([O III]), indicating that more data were needed to draw meaningful conclusions. In Figure 2, we show the relations between T_e ([N II]), T_e ([O II]), and T_e ([S II]) with respect to T_e ([O III]) obtained from the data presented in this paper and those of NGC 5253 (López-Sánchez et al. 2007), 30 Doradus (Peimbert 2003), NGC 5471 (Esteban et al. 2002), and the compilation of data for a sample of Galactic H II regions of García-Rojas & Esteban (2007). These data have been included because they are also based on high-spatial resolution spectroscopy (except in the cases of NGC 5447 and NGC 5471, where intermediate-resolution spectroscopy was used) and they have been analyzed in the same manner as the present sample, using the same atomic dataset and considering the recombination contribution to both the [N II] and [O II] line intensities. In the figure, we can see a rather clear linear relation between T_e ([N II]) with respect to T_e ([O III]), which is a substantial improvement with respect to the previous results by Kennicutt et al. (2003). Our least-squares fit to the points –weighted by their observational errors– of the T_e ([N II]) vs. T_e ([O III]) diagram gives:

$$T_e(\text{[N II]}) = 0.71 \times T_e(\text{[O III]}) + 3050 \text{ K,} \quad (3)$$

with a correlation coefficient of 0.91. It is remarkable that this empirical relation is almost identical to the theoretically predicted relationship from Garnett (1992), confirming that

the use of Garnett’s relation between these two indicators is entirely reliable (the same conclusion has been drawn by Bresolin et al. 2009). This is a result of special interest because while $T_e([\text{O III}])$ usually cannot be derived in metal-rich H II regions –where the $[\text{O III}] \lambda 4363$ auroral line becomes very faint– $T_e([\text{N II}])$ can be more easily determined from optical spectra (see Bresolin 2006), and shows a very weak dependence on n_e .

The apparent lack of consistency between $T_e([\text{O II}])$ and $T_e([\text{O III}])$ found by all the authors that have studied the empirical relation of these temperature indicators (Kennicutt et al. 2003; Pérez-Montero & Díaz 2003; Hägele et al. 2006, 2008) is remarkable. Kennicutt et al. (2003) proposed several possible sources of such inconsistency: a) the recombination contribution to $[\text{O II}]$ line intensity, b) the large contribution of collisional de-excitation to the $[\text{O II}]$ line ratios –dependence on n_e – used for deriving $T_e([\text{O II}])$, which is more important than for the rest of the indicators, except $T_e([\text{S II}])$, c) radiative transfer effects, d) observational uncertainties in the interstellar reddening, e) contamination by OH airglow emission of the $[\text{O II}]$ multiplet around 7325 Å. Pérez-Montero & Díaz (2003) and Hägele et al. (2006, 2008) obtain also a large scatter in their $T_e([\text{O II}])$ vs. $T_e([\text{O III}])$ diagrams, that include a large number of data points from the literature. These authors indicate that the scatter is probably due to the dependence of $T_e([\text{O II}])$ on electron density. However, our results shown in Figure 2 indicate a tighter and rather linear relation between $T_e([\text{O II}])$ and $T_e([\text{O III}])$. The least-squares fit gives:

$$T_e([\text{O II}]) = 0.99 \times T_e([\text{O III}]) + 410 \text{ K}, \quad (4)$$

with a correlation coefficient of 0.88, indicating that the use of Garnett’s relationship between $T_e([\text{O II}])$ and $T_e([\text{O III}])$ seems to be a reasonable approximation. It is important to remark that our data have been corrected for the recombination contribution to $[\text{O II}]$ –as also done by Pérez-Montero & Díaz (2003); Hägele et al. (2006, 2008)– and that the use of high spectral-resolution spectra precludes the contamination by OH airglow emission of the red $[\text{O II}]$ lines. The comparison of our result with the previous ones from the literature is puzzling. Considering that most of the scatter shown in the $T_e([\text{O II}])$ vs. $T_e([\text{O III}])$ diagrams of Pérez-Montero & Díaz (2003) and Hägele et al. (2006, 2008) should be due to the inclusion of inhomogeneous data points from the literature, we think that the sensitivity of $T_e([\text{O II}])$ to many different factors makes the statistical use of this indicator ill-advised when using inhomogeneous datasets.

As it can be seen in Figure 2, the third relationship studied: $T_e([\text{S II}])$ vs. $T_e([\text{O III}])$ shows a somewhat different behaviour than the previous ones. The data points show a larger scatter and the least-squares fit gives:

$$T_e([\text{S II}]) = 0.33 \times T_e([\text{O III}]) + 5015 \text{ K}, \quad (5)$$

with a correlation coefficient of 0.53, lower than in the previous cases. A large scatter in this relation is also evident in the data obtained by Pérez-Montero & Díaz (2003) and Hägele et al. (2008). A common result of these works is that $T_e([\text{S II}])$ is smaller than $T_e([\text{O II}])$ in most cases, in agreement with our results. There are several arguments to explain this behavior: a) due to the lower ionization potential of neutral sulphur, the zone of S^+ should not coincide with the zone where N^+ and O^+ are present –which are essentially cospatial– and this may be reflected in somewhat different temperatures in both zones, b) the contribution of $[\text{S II}]$ emission from diffuse ionized gas due to photon leakage from the H II region, c) the dependence of $T_e([\text{S II}])$ on electron density, d) some recombination contribution to $[\text{S II}]$ line intensities.

4.2. Ionic Abundances from CELs and RLs

Ionic abundances of N^+ , O^+ , O^{++} , Ne^{++} , S^+ , S^{++} , Cl^{++} , Cl^{3+} , Ar^{++} , and Ar^{3+} have been derived from CELs by making use of the IRAF task `ionic` of the package NEBULAR. We have assumed a two-zone scheme adopting $T_e([\text{N II}])$ for ions with a low ionization potential (N^+ , O^+ , and S^+) and $T_e([\text{O III}])$ for ions with a high ionization potential (O^{++} , Ne^{++} , S^{++} , Cl^{++} , Cl^{3+} , Ar^{++} , and Ar^{3+}). All the ionic abundances are included in Tables 6–8. We have used neither $T_e([\text{O II}])$ nor $T_e([\text{S II}])$ for the abundance determinations. As discussed in §§ 4.1, the $T_e([\text{O II}])$ may be affected by several sources of uncertainty and, in principle, may be a less confident temperature indicator. On the other hand, as we pointed out in §§ 4.1, $T_e([\text{S II}])$ is somewhat lower than $T_e([\text{N II}])$ or $T_e([\text{O II}])$ in most of the objects. This effect has been reported previously in several Galactic H II regions (García-Rojas et al. 2005, 2006, 2007), and might be produced by the presence of a temperature stratification in the outer zones of the nebulae or, conversely, by uncertainties in the atomic parameters of the ion. The H II region at the center of M 83 is the only object without a direct determination of $T_e([\text{O III}])$. For the abundance determinations adopted for this nebula we have assumed $T_e([\text{O III}]) = T_e([\text{N II}])$. The use of either the theoretical or the empirical relationships between $T_e([\text{O III}])$ and $T_e([\text{N II}])$ shown in equations 2 or 3 provides a value of $T_e([\text{O III}])$ of about 2900 K, which gives unreasonably high abundances, for example $12+\log(\text{O}^{++}/\text{H}^+) = 9.72$ or even $12+\log(\text{Ne}^{++}/\text{H}^+) = 10.22$. As it has been demonstrated by Stasińska (1978, 2005), high-metallicity –and low-temperature– H II regions may have large temperature gradients that could produce differences between the electron temperatures determined from line intensity ratios and the mean ionic temperatures (those obtained from photoionization models and used to derive the equations obtained by Garnett 1992). This effect can naturally explain the inappropriateness of the $T_e([\text{O III}])$ estimated for the H II region at the center of M 83.

Table 6. Ionic and Total Abundances^a

	NGC 595		NGC 604		H1013		NGC 5461		NGC 5447	
	$t^2 = 0.000$	$t^2 = 0.036$	$t^2 = 0.000$	$t^2 = 0.034$	$t^2 = 0.000$	$t^2 = 0.037$	$t^2 = 0.000$	$t^2 = 0.014$	$t^2 = 0.000$	$t^2 = 0.032$
Ionic Abundances from Collisionally Excited Lines										
N ⁺	7.13±0.02	7.28±0.06	6.82±0.03	6.94±0.04	7.35±0.04	7.52±0.11	6.85±0.04	6.89±0.06	6.43±0.05	6.51±0.05
O ⁺	8.27±0.03	8.44±0.06	7.92±0.04	8.06±0.05	8.23±0.06	8.43±0.13	7.80±0.06	7.85±0.08	7.57±0.11	7.66±0.11
O ⁺⁺	7.99±0.06	8.33±0.07	8.19±0.03	8.45±0.04	8.06±0.12	8.42±0.12	8.29±0.03	8.38±0.07	8.27±0.02	8.46±0.06
Ne ⁺⁺	6.73±0.08	7.11±0.16	7.27±0.03	7.56±0.08	7.01±0.16	7.41±0.36	7.46±0.04	7.56±0.11
S ⁺	5.50±0.02	5.65±0.06	5.47±0.03	5.59±0.04	5.63±0.04	5.80±0.11	5.34±0.04	5.38±0.06	5.23±0.05	5.31±0.05
S ⁺⁺	6.88±0.23	7.29±0.40	6.76±0.06	6.86±0.12	6.58±0.06	6.79±0.12
Cl ⁺⁺	4.80±0.06	5.12±0.13	4.58±0.03	4.83±0.07	4.72±0.12	5.07±0.27	4.59±0.04	4.68±0.10	4.55±0.04	4.73±0.09
Ar ⁺⁺	6.14±0.06	6.42±0.12	6.04±0.03	6.26±0.06	6.15±0.12	6.45±0.23	6.09±0.05	6.16±0.09	6.02±0.04	6.18±0.08
Ar ³⁺	4.20±0.10	4.29±0.14	4.26±0.05	4.45±0.10
Fe ⁺⁺	5.18±0.17	5.34±0.18	5.34±0.09	5.48±0.09	5.55±0.18	5.73±0.19	5.55±0.18	5.60±0.18	5.38±0.29	5.47±0.30
Ionic Abundances from Recombination Lines										
He ⁺	10.834±0.004	10.830±0.04	10.869±0.005	10.866±0.005	10.86±0.01	10.86±0.01	10.86±0.01	10.86±0.01	10.90±0.02	10.88±0.02
He ⁺⁺	7.80±0.11
C ⁺⁺	8.07±0.12	...	8.19±0.11	...	8.40±0.12	...	8.13±0.20	...	8.06±0.11	...
O ⁺⁺	8.33±0.07	...	8.45±0.04	...	8.42±0.11	...	8.38±0.07	...	8.46±0.07	...
Total Abundances										
He	10.849±0.004	10.845±0.004	10.887±0.005	10.884±0.005	10.87±0.01	10.87±0.01	10.88±0.01	10.88±0.01	10.90±0.02	10.88±0.02
C	8.53±0.12	...	8.40±0.11	...	8.67±0.12	...	8.30±0.20	...	8.20±0.12	...
N	7.31±0.05	7.53±0.10	7.28±0.05	7.49±0.07	7.57±0.10	7.82±0.19	7.46±0.08	7.54±0.11	7.21±0.12	7.38±0.13
O	8.45±0.03	8.69±0.05	8.38±0.02	8.60±0.03	8.45±0.06	8.73±0.09	8.41±0.03	8.49±0.06	8.35±0.02	8.52±0.06
Ne	7.19±0.10	7.47±0.19	7.46±0.05	7.70±0.10	7.41±0.21	7.72±0.42	7.59±0.06	7.67±0.15
S	6.91±0.23	7.31±0.48	6.86±0.06	6.93±0.12	6.72±0.06	6.88±0.12
Ar	6.38±0.08	6.60±0.13	6.22±0.03	6.47±0.07	6.35±0.14	6.62±0.24	6.12±0.05	6.19±0.09	6.04±0.04	6.20±0.08
Fe	5.34±0.19	5.55±0.21	5.73±0.10	5.94±0.11	5.74±0.23	5.98±0.26	6.08±0.20	6.15±0.21	6.06±0.33	6.23±0.35

^aIn units of $12+\log(X^{+m}/H^+)$.

Table 7. Ionic and Total Abundances^a

	VS 24	VS 38	VS 44		NGC 2363		K932	
	$t^2 = 0.000$	$t^2 = 0.000$	$t^2 = 0.000$	$t^2 = 0.039$	$t^2 = 0.000$	$t^2 = 0.120$	$t^2 = 0.000$	$t^2 = 0.033$
Ionic Abundances from Collisionally Excited Lines								
N ⁺	7.07±0.04	6.97±0.05	6.90±0.03	7.04±0.05	5.20±0.06	5.43±0.07	6.85±0.02	6.96±0.03
O ⁺	8.09±0.05	8.03±0.08	7.97±0.04	8.13±0.05	6.53±0.09	6.77±0.05	7.83±0.03	7.95±0.04
O ⁺⁺	8.05±0.06	7.93±0.04	8.13±0.03	8.43±0.06	7.73±0.02	8.02±0.05	8.28±0.02	8.52±0.04
Ne ⁺⁺	6.93±0.09	6.93±0.06	7.16±0.04	7.49±0.11	6.92±0.02	7.23±0.07	7.51±0.03	7.77±0.07
S ⁺	5.52±0.04	5.55±0.05	5.49±0.03	5.63±0.05	4.34±0.06	4.56±0.07	5.28±0.02	5.39±0.03
S ⁺⁺	6.73±0.12	6.37±0.09	6.73±0.06	7.07±0.11	5.70±0.03	6.01±0.08	6.76±0.04	7.03±0.07
Cl ⁺⁺	4.58±0.07	4.25±0.07	4.54±0.04	4.83±0.09	3.59±0.02	3.87±0.07	4.61±0.03	4.84±0.06
Cl ³⁺	3.84±0.18	4.12±0.14
Ar ⁺⁺	5.97±0.06	5.88±0.05	6.00±0.04	6.25±0.08	5.19±0.03	5.44±0.06	6.10±0.03	6.30±0.05
Ar ³⁺	4.73±0.02	5.03±0.07	3.89±0.08	4.14±0.08
Fe ⁺⁺	5.47±0.17	5.36±0.31	5.56±0.09	5.72±0.09	4.36±0.23	4.58±0.21	5.21±0.07	5.32±0.07
Fe ³⁺	5.02±0.21	5.23±0.22
Ionic Abundances from Recombination Lines								
He ⁺	10.820±0.007	10.881±0.006	10.848±0.006	10.833±0.006	10.88±0.01	10.85±0.01	10.911±0.005	10.907±0.005
He ⁺⁺	8.34±0.02
C ⁺⁺	8.15±0.24	8.27±0.15	7.98±0.18	...	7.55±0.09	...	8.31±0.13	...
O ⁺⁺	<8.50	<8.54	8.43±0.06	...	8.02±0.05	...	8.52±0.04	...
Total Abundances								
He	10.841±0.007	10.902±0.006	10.863±0.006	10.848±0.006	10.88±0.01	10.85±0.01	10.920±0.005	10.916±0.005
C	8.46±0.24	8.50±0.15	8.32±0.18	...	7.75±0.09	...	8.46±0.13	...
N	7.35±0.07	7.23±0.11	7.29±0.05	7.52±0.08	6.43±0.07	6.70±0.10	7.44±0.04	7.63±0.06
O	8.37±0.04	8.29±0.05	8.36±0.02	8.61±0.04	7.76±0.02	8.04±0.05	8.41±0.02	8.62±0.03
Ne	7.25±0.11	7.29±0.09	7.39±0.06	7.67±0.13	6.95±0.03	7.25±0.10	7.64±0.04	7.88±0.09
S	6.77±0.11	6.45±0.08	6.79±0.06	7.12±0.11	5.98±0.03	6.28±0.07	6.85±0.04	7.12±0.07
Ar	6.14±0.06	6.06±0.07	6.16±0.04	6.44±0.08	5.32±0.02	5.58±0.05	6.13±0.04	6.32±0.05
Fe	5.71±0.19	5.58±0.35	5.89±0.10	6.13±0.12	5.44±0.24	5.71±0.23	5.71±0.08	5.90±0.09

^aIn units of $12+\log(X^{+m}/H^+)$.

The errors in the ionic abundances shown in tables 6–8 have been computed as the quadratic sum of the independent contributions of n_e , T_e , and line flux uncertainties. We have considered two sets of abundances, one for $t^2 = 0$ and one for $t^2 > 0$ (see §§ 5.1).

[Fe II] lines have been detected in the spectra of some of our sample objects. Unfortunately, these lines are severely affected by continuum fluorescence effects (see Rodríguez 1999; Verner et al. 2000) and are not suitable for abundance determinations. [Fe III] lines have been detected in all the objects except at the nucleus of M83. For the calculations of the $\text{Fe}^{++}/\text{H}^+$ ratio, we have used a 34-level model atom that uses collision strengths from Zhang (1996) and the transition probabilities of Quinet (1996) as well as the new transitions found by Johansson et al. (2000). The adopted values of the $\text{Fe}^{++}/\text{H}^+$ abundance correspond to the mean of the abundances obtained for the different [Fe III] lines measured for each object. Several [Fe IV] lines have been detected in NGC 2363. The $\text{Fe}^{3+}/\text{H}^+$ ratio has been derived using a 33-level model atom where all collision strengths are those calculated by Zhang & Pradhan (1997) and the transition probabilities are those recommended by Froese Fischer et al. (2008).

We have measured several He I emission lines in the spectra of the sample objects. These lines arise mainly from recombination, but they can be affected by collisional excitation and self-absorption effects. We have used the effective recombination coefficients of Storey & Hummer (1995) for H I and those computed by Porter et al. (2005), with the interpolation formulae provided by Porter et al. (2007) for He I. The collisional contribution was estimated from Sawey & Berrington (1993) and Kingdon & Ferland (1995), and the optical depth in the triplet lines were derived from the computations by Benjamin et al. (2002). We have not corrected the He I lines for underlying stellar absorption because: (a) the use of high-spectral resolution data; (b) the lack of appropriate determinations of He I EWs in absorption for OB associations and for all the brightest He I lines along the optical spectrum (see Kennicutt et al. 2003). We have determined the He^+/H^+ ratio for $t^2 = 0$ and $t^2 > 0$ from a maximum likelihood method (Peimbert et al. 2000, 2002). The He II $\lambda 4686$ line has been detected in three objects: NGC 5461, NGC 2363, and NGC 4861. We have determined the $\text{He}^{++}/\text{H}^+$ ratio using the line emissivities calculated by Hummer & Storey (1987) and Storey & Hummer (1995). We have not calculated the $\text{He}^{++}/\text{H}^+$ ratios for $t^2 > 0$ considering the small effect of temperature fluctuations on this abundance and the negligible contribution of this ion to the total He/H ratio.

The high signal-to-noise of the spectra has permitted to detect and measure pure RLs of O II and C II in many of the sample objects. These lines have almost the same T_e and n_e dependence as H I lines. This almost eliminates the bias in the derived abundances in the case of line-of-sight temperature variations, with respect to abundances derived from CELs.

Let $I(\lambda)$ be the intensity of a RL of an element X, i times ionized, at wavelength λ ; then the abundance of the ionization state $i + 1$ of element X is given by

$$\frac{N(X^{i+1})}{N(H^+)} = \frac{\lambda(\text{\AA}) \alpha_{eff}(H\beta)}{4861 \alpha_{eff}(\lambda)} \frac{I(\lambda)}{I(H\beta)}, \quad (6)$$

where $\alpha_{eff}(\lambda)$ and $\alpha_{eff}(H\beta)$ are the effective recombination coefficients for the line and for H β , respectively. The $\alpha_{eff}(H\beta)/\alpha_{eff}(\lambda)$ ratio is almost independent of the adopted temperatures and densities.

Following Esteban et al. (1998), we have determined the O⁺⁺ abundances from the estimated total intensity of the RLs of multiplet 1 of O II. This last quantity is obtained by multiplying the sum of the intensities of the individual lines of multiplet 1 of O II observed in a given object by the multiplet correction factor, defined as:

$$m_{cf} = \frac{\sum_{all} s_{ij}}{\sum_{obs} s_{ij}}, \quad (7)$$

where s_{ij} are the theoretical line strengths, which are constructed assuming that they are proportional to the populations of their parent levels, if we assume LTE computations predictions. The upper sum runs over *all* the lines of the multiplet, and the lower sum runs over the *observed* lines of the multiplet. The lines of multiplet 1 of O II are not in LTE for densities $n_e < 10,000 \text{ cm}^{-3}$ (Ruiz et al. 2003; Tsamis et al. 2003). We have used the prescriptions given by Peimbert et al. (2005) to calculate the appropriate corrections for the relative strengths between the individual lines of multiplet 1. The O⁺⁺ and C⁺⁺ abundances from RLs have been calculated using the representative T_e -values of these ions, $T_e([O \text{ III}])$, and the effective recombination coefficients that are available in the literature (Storey 1994 for O II assuming LS coupling, and Davey et al. 2000 for C II). In the case of those objects where only upper limits of the O II $\lambda 4549$ intensity have been estimated, the corresponding upper limit of the O⁺⁺ abundance has been derived from the intensity of that line and the prescription given by Peimbert et al. (2005) for O II $\lambda 4549$.

4.3. Total Abundances

To derive the total gas-phase abundances of the different elements present in our spectra, we have to correct for the unseen ionization stages by using a set of ionization correction factors (ICFs). The total helium abundance has been corrected for the presence of neutral helium using the ionization fractions obtained from the photoionization models of Stasińska (1990) that reproduce the O abundance, O⁺⁺/O⁺ ratio, $T_e([O \text{ III}])$, and $T_e([N \text{ II}])$ measured in each object. In the case of M83, we have not determined the total He abundance due to

the low ionization degree of the nebula, that implies a large contribution of neutral helium and a very uncertain ICF. In the cases of NGC 5461, NGC 2363, and NGC 4861 –whose spectra show a rather faint He II $\lambda 4686$ line– we have assumed that the total He/H ratio is just the sum of He^+/H^+ and a small contribution of $\text{He}^{++}/\text{H}^+$, i.e. the amount of neutral helium is negligible inside these nebulae.

For C we have adopted an ICF-value for the presence of C^+ obtained from the photoionization models by Garnett et al. (1999). This correction seems to be fairly appropriate considering the relatively high ionization degree of the objects where the C II $\lambda 4267$ line has been detected. In order to derive the total abundance of nitrogen we have used the usual ICF based on the similarity between the ionization potential of N^+ and O^+ (Peimbert & Costero 1969) in all the cases. Due to the absence of the He II $\lambda 4686$ line in most of the objects, the total abundance of oxygen has been calculated as the sum of O^+ and O^{++} abundances. We decided to make the same approximation in the cases of NGC 5461, NGC 2363, and NGC 4861 due to the weakness of the He II $\lambda 4686$ line detected in these objects, which implies an irrelevant contribution of O^{3+} .

The only measurable CELs of Ne in the optical range are those of Ne^{2+} but the fraction of Ne^+ may be important in the nebula. For this element, we have adopted the usual expression proposed by Peimbert & Costero (1969) that assumes that the ionization structure of Ne is similar to that of O. We have measured CELs of two ionization stages of S: S^+ and S^{2+} , and used the ICF proposed by Stasińska (1978) –which is based on photoionization models of H II regions– to take into account the presence of S^{3+} . For argon we have determinations of the Ar^{2+} abundance for all the objects and also of the Ar^{3+} abundance for NGC 5461, NGC 5447, NGC 2363, K932, and NGC 4861. However, some contribution of Ar^+ is expected. We have adopted the ICF recommended by Izotov et al. (1994) for this element.

Finally, for iron, we have determined the Fe^{++} abundance for all the objects and also the Fe^{3+} abundance for NGC 2363. Some small contribution of Fe^+ should be present, mainly in the nebulae of lower ionization degree. We have used an ICF scheme based on photoionization models of Rodríguez & Rubin (2005) to obtain the total Fe/H ratio using the Fe^{++} abundances.

In Tables 6–8 we show the total abundances for $t^2 = 0$ and for the t^2 -value adopted in those objects where this parameter was estimated (see §§ 5.1).

Table 8. Ionic and Total Abundances^a

	NGC 1741	NGC 4395-70	NGC 4861	M 83
Ionic Abundances from Collisionally Excited Lines				
N ⁺	6.72±0.09	6.35±0.26	5.70±0.13	8.48±0.09
O ⁺	7.77±0.14	7.53±0.24	7.19±0.24	8.94±0.09
O ⁺⁺	8.30±0.07	7.95±0.06	7.98±0.02	7.79±0.12
Ne ⁺⁺	7.53±0.10	7.24±0.07	7.24±0.02	7.76±0.24
S ⁺	5.64±0.08	5.59±0.22	4.89±0.12	6.76±0.08
S ⁺⁺	6.75±0.14	6.38±0.11	6.23±0.03	6.76±0.08
Cl ⁺⁺	...	4.32±0.11	4.07±0.04	...
Ar ⁺⁺	5.98±0.08	5.76±0.06	5.60±0.02	6.10±0.12
Ar ³⁺	4.55±0.02	...
Fe ⁺⁺	5.68±0.19	5.70±0.30	5.18±0.21	...
Ionic Abundances from Recombination Lines				
He ⁺	10.72±0.02	10.82±0.02	10.90±0.01	10.58±0.02
He ⁺⁺	8.73±0.03	...
C ⁺⁺	<7.97	<7.47	<7.49	...
O ⁺⁺	<8.68	<8.72	<8.25	...
Total Abundances				
He	10.73±0.02	10.83±0.02	10.91±0.01	...
N	7.36±0.18	6.56±0.28	6.56±0.28	8.51±0.15
O	8.41±0.06	8.09±0.15	8.05±0.04	8.97±0.08
Ne	7.64±0.14	7.38±0.17	7.30±0.04	8.94±0.30
S	6.89±0.13	6.51±0.10	6.40±0.03	7.42±0.23
Ar	6.23±0.11	5.98±0.23	5.65±0.02	...
Fe	5.95±0.25	5.97±0.42	5.45±0.33	...

^aIn units of $12+\log(X^{+m}/H^+)$.

Table 9. Comparison of Ionic Abundances^a and t^2 Parameter

Object	O ⁺⁺ /H ⁺		ADF(O ⁺⁺)	t^2 (O ⁺⁺)	C ⁺⁺ /H ⁺		ADF(C ⁺⁺)	t^2 (C ⁺⁺)	t^2 (He ⁺)
	CELs	RLs			CELs	RLs			
NGC 595	7.99±0.06	8.33±0.07	0.34±0.08	0.036±0.012	...	8.07±0.12	0.033±0.009
NGC 604	8.19±0.02	8.45±0.04	0.26±0.04	0.034±0.008	...	8.19±0.11	0.022±0.010
H1013	8.06±0.12	8.42±0.11	0.36±0.13	0.037±0.020	...	8.40±0.12	0.031±0.017
NGC 5461	8.29±0.03	8.38±0.07	0.09±0.08	0.014±0.014	8.27 ^b /7.90 ^c	8.13±0.20	-0.14/0.23	<0/0.028	0.057±0.018
NGC 5447	8.27±0.02	8.46±0.07	0.19±0.07	0.032±0.007	...	8.06±0.11	0.094±0.034
VS 24	8.05±0.06	<8.50	<0.45	8.15±0.24	0.075±0.012
VS 38	7.93±0.04	<8.54	<0.61	...	8.00 ^b /7.84 ^c	8.27±0.15	0.27/0.43	0.026/0.035	0.057±0.015
VS 44	8.13±0.03	8.43±0.06	0.30±0.06	0.039±0.010	8.08 ^b /7.85 ^c	7.98±0.18	-0.10/0.13	<0/0.018	0.066±0.010
NGC 2363	7.73±0.02	8.02±0.05	0.29±0.05	0.120±0.022	7.15 ^d	7.55±0.09	0.40	0.153	0.101±0.019
K932	8.28±0.02	8.52±0.04	0.24±0.04	0.033±0.007	...	8.31±0.13	0.030±0.009
NGC 1741	8.30±0.07	<8.68	<0.38	<7.97	0.035±0.076
NGC 4395-70	7.95±0.06	<8.72	<0.77	<7.47	0.125±0.064
NGC 4861	7.98±0.02	<8.25	<0.27	...	7.44±0.11 ^e	<7.49	<0.05	...	0.103±0.020
M 83	7.79±0.12	0.036±0.010

^aIn units of $12+\log(X^{+m}/H^+)$.

^bGarnett et al. (1999), assuming $R_V = 3.1$.

^cGarnett et al. (1999), assuming $R_V = 5$.

^dGarnett et al. (1995).

^eKobulnicky & Skillman (1998).

5. Discussion

5.1. The Abundance Discrepancy Factor in the Sample Objects

In Table 9, we include the O^{++} and C^{++} abundances determined from RLs and CELs for the sample objects as well as the ADF for each ion. The C^{++} abundance determinations based on CELs included in the table have been calculated from the intensities of [C III] $\lambda 1907 + C\text{ III] } \lambda 1909$ lines, which are in the UV and come from the literature (Garnett et al. 1995, 1999; Kobulnicky & Skillman 1998). Except in the cases of NGC 2363 and NGC 4861, the rest of the C^{++}/H^+ ratios based on CELs have two possible values, which correspond to the higher and lower limits adopted by Garnett et al. (1999) because of the uncertainty in the choice of the UV reddening function from their data. Garnett et al. (1995) determined the C^{++} abundance of NGC 2363 from UV CELs, and because of its low reddening, the uncertainty in the UV reddening function is not a concern for this object. In the case of NGC 4861, the choice of the UV reddening law can also affect but not very importantly because its relatively low extinction (see Kobulnicky & Skillman 1998).

As it can be seen in Table 9, the values of the $ADF(O^{++})$ are remarkably similar in all the objects, with a mean value of 0.26 ± 0.09 dex, which is very similar to the mean $ADF(O^{++})$ obtained for a sample of Galactic H II regions (see García-Rojas & Esteban 2007, and references therein) and for other EHRs (0.30 ± 0.09 dex, see López-Sánchez et al. 2007, and references therein). The upper limits of the $ADF(O^{++})$ included in Table 9 are always of the order or larger than the mean $ADF(O^{++})$. In the case of the $ADF(C^{++})$ the results are not so clear because of the limited number of determinations available in the literature, aperture effects, and the uncertainty in the UV reddening function assumed to derive the abundance from UV CELs, however, our values of the $ADF(C^{++})$ for NGC 2363 and those corresponding to $R_V = 5.0$ for NGC 5461, VS 38, and VS 44 are fairly similar to the $ADF(C^{++})$ -values compiled by López-Sánchez et al. (2007) for other Galactic and extragalactic H II regions. In the case of NGC 4861 we find a puzzling result because its upper limit of the $ADF(C^{++})$ is about zero.

As a conclusion of all the results about the ADF-values gathered in this and previous papers by our group, the ADF seems to be a remarkably constant quantity in H II regions. It seems clear that whatever phenomenon produces this discrepancy, it does not depend on the metallicity of the H II region, nor on its galactocentric distance –when the region belongs to a spiral galaxy– nor on the morphological type (or the absolute magnitude) of the host galaxy. This is a fairly different behavior from the one shown by the ADF in PNe, where this parameter changes almost by one order of magnitude from one object to the other. The results of this paper reinforce the suggestion of García-Rojas & Esteban (2007) that the

physical mechanism that produces the abundance discrepancy –or the bulk of it– in the PNe with large ADF-values should be different to that acting in H II regions.

Assuming the validity of the temperature fluctuations paradigm and that this phenomenon produces the abundance discrepancy, we can estimate the values of the t^2 parameter for each object. In Table 9, we include the t^2 -values that produce the agreement between the abundance determinations obtained from CELs and RLs of O^{++} and C^{++} . These calculations have been made following the formalism outlined by Peimbert & Costero (1969). As we have indicated along the paper, the ionic abundances, ICFs, and total abundances have been calculated considering both possibilities: $t^2 = 0$ and the t^2 -values obtained from the $ADF(O^{++})$. We have assumed that the same t^2 is valid for determining the abundances of the different ionic species. As we expect from the similarity of the $ADF(O^{++})$ found for the sample objects, the corresponding values of the t^2 parameter obtained are also fairly similar, and also similar to those obtained for Galactic H II regions and other EHRs (see García-Rojas & Esteban 2007; López-Sánchez et al. 2007). It is also interesting to note that the t^2 -value determined from the $ADF(C^{++})$ for NGC 2363 is consistent with that determined from the $ADF(O^{++})$. For the rest of the sample objects where the $ADF(C^{++})$ has been estimated, a firm conclusion cannot be drawn due to the strong dependence of the associated t^2 -value on the assumed UV reddening law. In Table 9, we also include the t^2 -values obtained from the application of a maximum likelihood method (Peimbert et al. 2000, 2002) to search for the physical conditions, He^+/H^+ ratios, and optical depths that would be a simultaneous fit to the measured lines of He I (see §§ 4.2). As we can see in Table 9, the values of $t^2(He^+)$ and $t^2(O^{++})$ are consistent within the errors in the cases of NGC 595, H1013, NGC 2363, and K932 (50% of the objects where both quantities were determined), marginally consistent in the case of NGC 604, and in disagreement for NGC 5461, NGC 5447, and VS 44.

The results included in Table 9 are fairly consistent with previous determinations of the t^2 parameter for some of the sample objects. Esteban et al. (2002) obtained t^2 -values of 0.027 ± 0.018 , 0.041 ± 0.021 , and 0.128 ± 0.045 for NGC 604, NGC 5461, and NGC 2363, respectively, also from the $ADF(O^{++})$. In the case of NGC 2363, Esteban et al. (2002) obtain $t^2 \sim 0.102$ from the $ADF(C^{++})$. Interestingly, González-Delgado et al. (1994) estimate a $t^2 = 0.064 - 0.098$ from the independent method based on the comparison of $T_e([O III])$ and $T(Pac)$ (Paschen continuum) for NGC 2363. In the case of NGC 2363, it is remarkable that four independent methods for estimating t^2 give entirely consistent results. Finally, Bresolin (2007) obtains a $t^2 = 0.06 \pm 0.02$ for H 1013 from the comparison of $T_e([O III])$ and $T(Bac)$ (Balmer continuum).

Clearly, the fact that RLs and CELs provide abundances that differ by about 0.3 dex is an important concern in nebular astrophysics. An additional problem is that we do not know

which kind of lines gives the correct abundances. This situation means that the chemical composition of cosmic objects derived from H II regions are in a sort of quarantine and perhaps should be revised. This puzzling situation has important implications for different relevant astrophysical issues such as: (a) the ingredients of chemical evolution models and predicted stellar yields (see Carigi et al. 2005); (b) the luminosity- and mass-metallicity relations for local and high-redshift star-forming galaxies (see Salzer et al. 2005); (c) the calibration of strong-line methods for deriving H II region abundances (Peimbert et al. 2007); (d) the possible metallicity dependence of the Cepheid period-luminosity relation (Sakai et al. 2004); (e) the metallicity dependence of the number ratios of the different types of Wolf-Rayet stars (Meynet & Maeder 2005); (f) the comparison of the Solar abundances with the Orion Nebula abundances (Carigi & Peimbert 2008).

5.2. The C/H and C/O Radial Gradients in M 33, M 101, and NGC 2403

The determination of the O/H and/or C/H ratios from RLs in two or more H II regions in the spiral galaxies M 33, M 101, and NGC 2403 allows us to estimate the radial abundance gradients of those two elements in these galaxies. Considering the O and C abundances determined in this paper and the galactocentric distances and R/R_0 ratios compiled in Table 1, we have obtained the O/H (CELs), O/H (RLs), C/H (RLs) and C/O (RLs) gradients shown in Table 10. In the case of M 101, we have also included the data for NGC 5471 obtained by Esteban et al. (2002) for the gradient determinations. In Figure 3, we show the gradients found for M 101. It is remarkable the clear trend of the gradients found for this galaxy. For comparison, in Table 10 we also include the C and O gradients determined by Esteban et al. (2005) for the Milky Way. An important result in all the cases is that the slope of the O abundance gradients is very similar independently of the kind of line –RLs or CELs– used for the abundance calculation. This is a likely consequence of the lack of correlation between the ADF(O⁺⁺) and metallicity.

The O abundance gradients determined from CELs of these galaxies have been studied in detail by many authors, especially for M 33 and M 101. The values of the O/H ratio that we obtain from CELs for each individual H II region of these galaxies do not differ typically more than 0.1 or 0.2 dex from the values found in the literature. The largest differences are for VS 24 and VS 38 of NGC 2403. The O abundances found by Garnett et al. (1997) are higher than ours by a factor of 0.39 dex and 0.24 dex for VS 24 and VS 38, respectively, this can be due to the more uncertain data of those authors. In fact, Garnett et al. (1997) find a negative reddening coefficient for VS 24 –we obtain $c(H\beta) = 0.34$, a value more similar to those found for the rest of the H II regions observed in NGC 2403– and they do not obtain

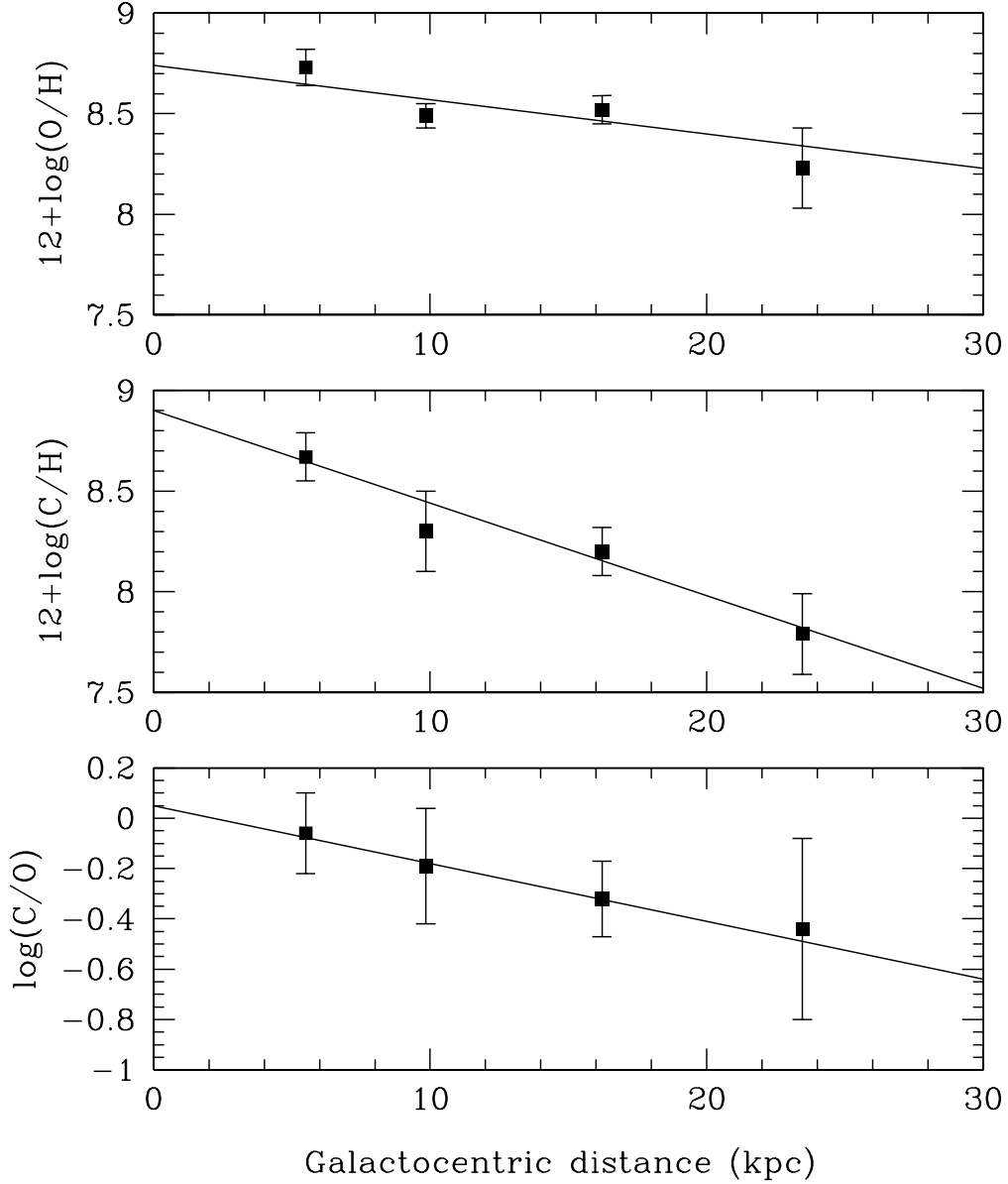


Fig. 3.— O, C, and C/O radial abundance gradients of the disk of the spiral galaxy M 101 from H II region abundances determined from recombination lines. The lines indicate the least-squares linear fits to the data. The point at $R_G = 23.45$ kpc corresponds to NGC 5471 and has been taken from Esteban et al. (2002).

a direct determination of $T_e([\text{O III}])$ for VS 38.

In the case of M 33, we obtain a slope of the O/H gradient that is flatter than that of Vílchez et al. (1988) (-0.12 ± 0.01 dex kpc^{-1}), steeper than those determined by Crockett et al. (2006) and Rosolowsky & Simon (2008) (values of -0.01 ± 0.01 and -0.03 ± 0.01 dex kpc^{-1} , respectively), but similar to those obtained by Urbaneja et al. (2005) –from the spectral analysis of B-type supergiant stars– and Magrini et al. (2007). For M 101, our O/H gradient is consistent with that of -0.029 ± 0.003 dex kpc^{-1} obtained by Kennicutt et al. (2003) and slightly flatter than that obtained by Esteban et al. (2002) from RLs of only two H II regions of the galaxy. However, our C/O gradient is somewhat steeper than the estimate of Esteban et al. (2002) but consistent with the value determined by Garnett et al. (1999) from CELs, which is between -0.025 and -0.040 , depending on the adopted UV reddening function. In the case of NGC 2403, our O/H (CELs) gradient is slightly positive but with a large uncertainty, in contrast to the negative gradients obtained by Fierro et al. (1986), Garnett et al. (1997), and van Zee et al. (1998), who find values between -0.07 and -0.10 . This result could be spurious and due to the narrow baseline of galactocentric distances covered with the three H II regions that we have observed in this galaxy.

As Esteban et al. (2005) found for the Milky Way, the C/H gradients are steeper than the ones obtained for the O/H ratio in all the galaxies, producing the negative slopes of the C/O gradients. Based on chemical evolution models of the Milky Way, Carigi et al. (2005) have found that such values of the slope of the C/O gradient can only be reproduced when carbon yields that increase with metallicity owing to stellar winds in massive stars are considered (as the yields obtained by Maeder 1992; Meynet & Maeder 2002; Hirschi et al. 2005). However, it is clear that tailored chemical evolution models for each individual spiral galaxy would be necessary in order to reach more precise conclusions on this issue.

A general correlation between C/O and O/H has been obtained by Garnett et al. (1995) and Garnett et al. (1999) from observations of CELs in dwarf irregular and spiral galaxies and by Esteban et al. (2002) from observations of RLs in a small sample of Galactic and extragalactic H II regions. In Figure 4 we have included the results for the EHRs observed in this paper and others from the literature (Esteban et al. 2002; Peimbert 2003; Peimbert et al. 2005; López-Sánchez et al. 2007) as well as the points corresponding to the sample of Galactic H II regions of García-Rojas (2006) and García-Rojas & Esteban (2007). As we can see in the figure, the Galactic objects and the H II regions belonging to spiral galaxies follow a rather clear trend, where the C/O ratio experiences a strong increase for O abundances between 8.5 and 8.8. This behaviour has also been observed in samples of nearby F and G dwarf stars of the Galactic disk (Bensby & Feltzing 2006) and dwarf and subgiant stars of the same spectral types belonging to the Galactic halo population (Akerman et al. 2004).

Bensby & Feltzing (2006) remark that the C/O vs. O/H trend is fairly similar to the well-known Fe/O vs. O/H one, suggesting that the low- and intermediate-mass stars should be important contributors to the C enrichment at higher metallicities. This was also one of the main results of the chemical evolution models by Carigi et al. (2005).

In Figure 4, we include the predictions of chemical evolution models for the present-day Galactic disk at different Galactocentric distances (Carigi & Peimbert 2008) that reproduce the observed C, O, and C/O gradients of the Galactic disk determined by Esteban et al. (2005). The solid line represents the results of a model that assumes the high-wind yields by Maeder (1992) and $M_{up} = 80 M_{\odot}$ (Carigi et al. 2005). The dashed line represents the results of a model that considers the low-wind yields by Hirschi et al. (2005) and $M_{up} = 80 M_{\odot}$ (Carigi & Peimbert 2008). In Figure 4, we can see that the predictions for high-wind yields match quite well the distribution of the points corresponding to the H II regions in the Milky Way and other spiral galaxies. This is an important result considering that the objects belong to spiral galaxies of different morphological type than the Milky Way, different masses, and different absolute magnitudes. This would imply that the assumptions used to generate the chemical evolution model of our Galaxy are reasonable for other spirals as well. In general, the O/H and C/O ratios of H II regions in dwarf galaxies are lower than those of the objects in spiral galaxies, and their C/O ratios also show a larger scatter. Garnett et al. (1999) indicated that changes in the assumed star formation law through its dependence on the power of the gas surface density can change the curves of the C/O vs. O/H relation in the C/O axis. This can be the case of dwarf galaxies with respect to the more massive spiral galaxies, since their gas consumption timescales must be very different and models for the Milky Way should not necessarily reproduce their chemical evolution.

The O and C abundances of the H II regions presented in Figure 4 have not been corrected for the fraction of atoms embedded in dust, the Fe/O ratio in the observed H II regions is at least one order of magnitude smaller than in the Sun implying that most of the Fe is trapped in dust grains. According to Esteban et al. (1998) and to Mesa-Delgado et al. (2009) the fraction of O and C embedded in dust grains in the Orion Nebula is about 0.1 dex. By assuming that some fraction of C and O is embedded in dust grains, the gas plus dust C/O values of the H II regions in Figure 4 would not be affected while the gas plus dust O/H values should be increased. An increase of the O/H ratios slightly lower than that estimated for the Orion Nebula (i.e. 0.05 dex) would produce a better agreement between the observations and the chemical evolution models with high-wind yields presented in this figure. At any rate, strong conclusions cannot be drawn from this comparison considering the large uncertainties in both the chemical evolution models and observations.

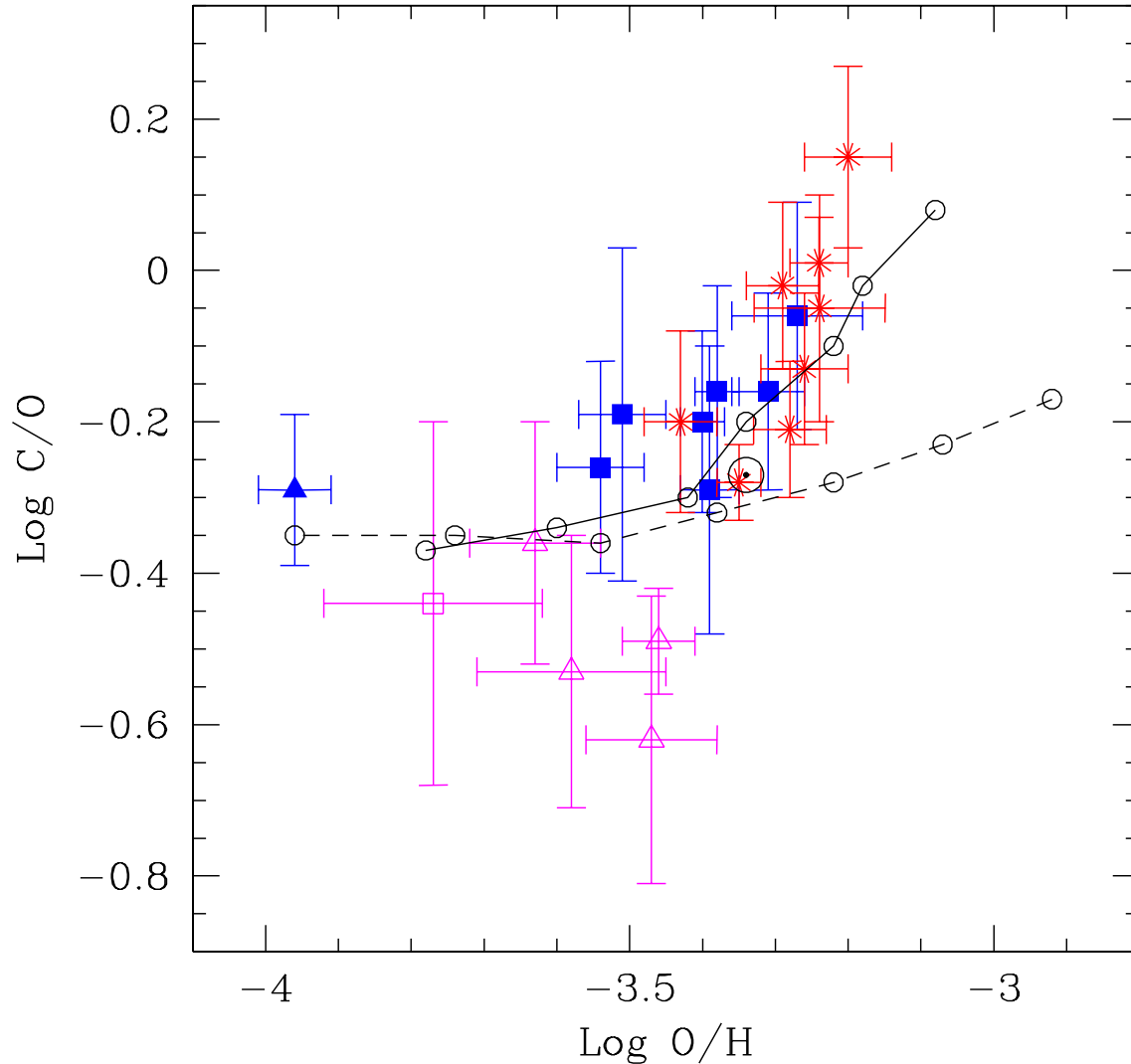


Fig. 4.— C/O vs. O/H ratios of Galactic and extragalactic H II regions (EHRs) determined from recombination lines. Filled (blue) symbols represent the data analysed in this paper; the filled squares correspond to abundance ratios of EHRs in spiral galaxies and the filled triangle to NGC 2363, an EHR in a dwarf galaxy. The empty (magenta) square corresponds to NGC 5471, an EHR at the outskirts of M 101 (data from Esteban et al. 2002). Empty (magenta) triangles correspond to data for EHRs in dwarf galaxies taken from the literature: 30 Dor (Peimbert 2003), region V of NGC 6822 (Peimbert et al. 2005), and regions A and C of NGC 5253 (López-Sánchez et al. 2007). The (red) asterisks correspond to data for Galactic H II regions (García-Rojas 2006; García-Rojas & Esteban 2007). The solar symbol (large circle) represents the abundances of the Sun (Grevesse et al. 2007). The lines show the predictions of chemical evolution models by Carigi et al. (2005) and Carigi & Peimbert (2008) for the present-day Galactic disk at different Galactocentric distances for high-wind yields and $M_{\text{exp}} = 80 M_{\odot}$ (solid line) and for low-wind yields and $M_{\text{exp}} = 80 M_{\odot}$ (dashed line).

6. Conclusions

Echelle spectrophotometry from 3550 to 7440 Å has been obtained with the HIRES spectrograph at the Keck I telescope for 13 extragalactic H II regions (EHRs). One additional object was observed with the WHT telescope at lower spectral resolution. The EHRs observed include objects in the spiral galaxies M 31, M 33, M 83, M 101, NGC 2403, and NGC 4395 as well as in irregular and blue compact dwarf galaxies: NGC 1741, NGC 2366, and NGC 4861.

The spectra are very deep and a number of lines between 38 and 135 have been measured in each EHR. We detected C II lines in 10 of the objects and O II lines in 8 of them. This allows us to derive the C⁺⁺ and O⁺⁺ abundances from recombination lines, which are independent of possible variations of the spatial distribution of the electron temperature in the nebulae.

We have obtained a large number of different T_e determinations, in particular those associated with low ionization potential ions: [N II], [O II], and [S II]. We have obtained a rather tight empirical linear relation between T_e ([N II]) and T_e ([O III]), which is almost identical to the relationship found by Garnett (1992) from photoionization models. The use of this relation is of interest for abundance determinations of H II regions where T_e ([O III]) can not be determined. A linear relationship is also found between T_e ([O II]) and T_e ([O III]) and between T_e ([S II]) and T_e ([O III]), but with a larger scatter in this last case.

The O⁺⁺ abundance determined from O II recombination lines is always larger than that determined from collisionally excited lines of [O III] in all the objects where both quantities have been calculated. The mean difference between both abundances –the so-called abundance discrepancy factor (ADF)– is 0.26 ± 0.09 dex –about a factor of 2, which is also similar to the typical values of this parameter in Galactic H II regions and EHRs from the literature. This result indicates that whatever mechanism is producing the abundance discrepancy in H II regions, it seems independent of the properties of the H II regions and of the parent galaxy.

We have determined the O/H, C/H, and C/O radial gradients in the spiral galaxies: M 33, M 101, and NGC 2403. We find that the C/H gradients are always steeper than those of O/H, producing negative slopes of the C/O gradient. The behavior of these gradients is similar to that of the Milky Way determined by Esteban et al. (2005), and can be reproduced when carbon yields that increase with metallicity owing to stellar winds in massive stars are considered (Carigi et al. 2005; Carigi & Peimbert 2008). The relation between C/O and O/H in extragalactic and Galactic H II regions shows a rather clear trend, where the C/O ratio shows a strong increase for O abundances between 8.5 and 8.8, indicating that the low-

and intermediate-mass stars should be important contributors to the C enrichment at higher metallicities.

We are grateful to the referee of this paper for his/her useful comments. This work has been funded by the Spanish Ministerio de Ciencia y Tecnología (MCyT) under project AYA2004-07466, Ministerio de Educación y Ciencia (MEC) under project AYA2007-63030, and the Mexican CONACyT grant 46904. F.B gratefully acknowledges the support from the NSF grant AST-0707911.

REFERENCES

- Akerman, C. J., Carigi, L., Nissen, P. E., Pettini, M., & Asplund, M. 2004, *A&A*, 414, 931
- Benjamin, R.A., Skillman, E.D. & Smits, D.P. 2002, *ApJ*, 569, 288
- Bensby, T., & Feltzing, S. 2006, *MNRAS*, 367, 1181
- Bresolin, F. 2006, arXiv:astro-ph/0608410
- Bresolin, F. 2007, *ApJ*, 656, 186
- Bresolin, F. 2008, *IAU Symposium*, 250, 273
- Bresolin, F., Gieren, W., Kudritzki, R.-P., Pietrzynski, G., Urbaneja, M., & Carraro, G. 2009, *ApJ*, submitted
- Bresolin, F., Schaerer, D., González Delgado, R. M., & Stasińska, G. 2005, *A&A*, 441, 981
- Campbell, A., Terlevich, R., & Melnick, J. 1986, *MNRAS*, 223, 811
- Carigi, L., & Peimbert, M. 2008, *Revista Mexicana de Astronomia y Astrofisica*, 44, 341
- Carigi, L., Peimbert, M., Esteban, C., & García-Rojas, J. 2005, *ApJ*, 623, 213
- Cedrés, B., & Cepa, J. 2002, *A&A*, 391, 809
- Conti, P. S., & Massey, P. 1981, *ApJ*, 249, 471
- Crockett, N. R., Garnett, D. R., Massey, P., & Jacoby, G. 2006, *ApJ*, 637, 741
- Davey, A. R., Storey, P. J., & Kisielius, R. 2000, *A&AS*, 142, 85
- de Vaucouleurs, G., de Vaucouleurs, A., & Corwin, H. G. 1976, *University of Texas Monographs in Astronomy*, Austin: University of Texas Press, 1976.

- de Vaucouleurs, G., de Vaucouleurs, A., Corwin, H. G., Jr., Buta, R. J., Paturel, G., & Fouque, P. 1991, Volume 1-3, XII, 2069 pp. 7 figs.. Springer-Verlag Berlin Heidelberg New York, 1991.
- Dinerstein, H. L., & Shields, G. A. 1986, *ApJ*, 311, 45
- Esteban, C., García-Rojas, J., Peimbert, M., Peimbert, A., Ruiz, M. T., Rodríguez, M., & Carigi, L. 2005, *ApJ*, 618, L95
- Esteban, C., Peimbert, M., García-Rojas, J., Ruiz, M. T., Peimbert, A., & Rodríguez, M. 2004, *MNRAS*, 355, 229
- Esteban, C., Peimbert, M., Torres-Peimbert, S., & Escalante, V. 1998, *MNRAS*, 295, 401
- Esteban, C., Peimbert, M., Torres-Peimbert, S., & Rodríguez, M. 2002, *ApJ*, 581, 241
- Fierro, J., Torres-Peimbert, S., & Peimbert, M. 1986, *PASP*, 98, 1032
- Freedman, W. L., et al. 2001, *ApJ*, 553, 47
- Froese Fischer, C., Rubin, R. H., & Rodríguez, M. 2008, *MNRAS*, 391, 1828
- Galarza, V. C., Walterbos, R. A. M., & Braun, R. 1999, *AJ*, 118, 2775
- García-Rojas, J. 2006, PhD thesis, Universidad de La Laguna
- García-Rojas, J., & Esteban, C. 2007, *ApJ*, 670, 457
- García-Rojas, J., Esteban, C., Peimbert, A., Peimbert, M., Rodríguez, M., & Ruiz, M. T. 2005, *MNRAS*, 362, 301
- García-Rojas, J., Esteban, C., Peimbert, A., Rodríguez, M., Peimbert, M., & Ruiz, M. T. 2007, *Rev. Mexicana Astron. Astrofis.*, 43, 3
- García-Rojas, J., Esteban, C., Peimbert, M., Costado, M. T., Rodríguez, M., Peimbert, A., & Ruiz, M. T. 2006, *MNRAS*, 368, 253
- García-Rojas, J., Esteban, C., Peimbert, M., Rodríguez, M., Ruiz, M. T., & Peimbert, A. 2004, *ApJS*, 153, 501
- Garnett, D. R. 1992, *AJ*, 103, 1330
- Garnett, D.R., Shields, G.A., Peimbert, M., Torres-Peimbert, S., Skillman, E.D., Dufour, R.J., Terlevich, E. & Terlevich, R.J. 1999, *ApJ*, 513, 168

- Garnett, D. R., Shields, G. A., Skillman, E. D., Sagan, S. P., & Dufour, R. J. 1997, *ApJ*, 489, 63
- Garnett, D. R., Skillman, E. D., Dufour, R. J., Peimbert, M., Torres-Peimbert, S., Terlevich, R., Terlevich, E., & Shields, G. A. 1995, *ApJ*, 443, 64
- Gil de Paz, A., Madore, B. F., & Pevunova, O. 2003, *ApJS*, 147, 29
- González-Delgado, R. M., et al. 1994, *ApJ*, 437, 239
- Grevesse, N., Asplund, M., & Sauval, A. J. 2007, *Space Science Reviews*, 130, 105
- Hägele, G. F., Pérez-Montero, E., Díaz, Á. I., Terlevich, E., & Terlevich, R. 2006, *MNRAS*, 372, 293
- Hägele, G. F., Díaz, Á. I., Terlevich, E., Terlevich, R., Pérez-Montero, E., & Cardaci, M. V. 2008, *MNRAS*, 383, 209
- Hickson, P. 1982, *ApJ*, 255, 382
- Hirschi, R., Meynet, G., & Maeder, A. 2005, *A&A*, 433, 1013
- Hodge, P. W., Gurwell, M., Goldader, J. D., & Kennicutt, R. C., Jr. 1990, *ApJS*, 73, 661
- Hummer, D. G., & Storey, P. J. 1987, *MNRAS*, 224, 801
- Izotov, Y.I., Thuan, T.X., & Lipovetski, 1994
- Johansson, S., Zethson, T., Hartman, H., Ekberg, J. O., Ishibashi, K., Davidson, K., & Gull, T. 2000, *A&A*, 361, 977
- Kamphuis, J. J. 1993, Ph.D. Thesis, Univ. Groningen
- Kennicutt, R. C., Jr., Bresolin, F., & Garnett, D. R. 2003, *ApJ*, 591, 801
- Kennicutt, R. C., Jr., & Garnett, D. R. 1996, *ApJ*, 456, 504
- Kingdon, J. & Ferland, G.J. 1995, *ApJ*, 442, 714
- Kobulnicky, H. A., & Skillman, E. D. 1998, *ApJ*, 497, 601
- Liu, X.-W. 2006, *Planetary Nebulae in our Galaxy and Beyond*, 234, 219
- Liu, X.-W., Storey, P. J., Barlow, M. J., Danziger, I. J., Cohen, M., & Bryce, M. 2000, *MNRAS*, 312, 585

- López-Sánchez, Á. R., Esteban, C., & García-Rojas, J. 2006, *A&A*, 449, 997
- López-Sánchez, A. R., Esteban, C., García-Rojas, J., Peimbert, M., & Rodríguez, M. 2007, *ApJ*, 656, 168
- López-Sánchez, Á. R., Esteban, C., & Rodríguez, M. 2004, *ApJS*, 153, 243
- Maeder, A. 1992, *A&A*, 264, 105
- Magrini, L., Vílchez, J. M., Mampaso, A., Corradi, R. L. M., & Leisy, P. 2007, *A&A*, 470, 865
- Mazzarella, J.M. & Boroson, T.A. 1993, *ApJS*, 85, 27
- McCall, M. L., Rybski, P. M., & Shields, G. A. 1985, *ApJS*, 57, 1
- Mesa-Delgado, A., Esteban, C., García-Rojas, J., Luridiana, V., Bautista, M., Rodríguez, M., López-Marín, L., & Peimbert, M. 2009, *MNRAS*, in press
- Meynet, G., & Maeder, A. 2002, *A&A*, 390, 561
- Meynet, G., & Maeder, A. 2005, *A&A*, 429, 581
- Peimbert, A. 2003, *ApJ*, 584, 735
- Peimbert, A., Peimbert, M. & Luridiana, V. 2002, *ApJ*, 565, 688
- Peimbert, A., Peimbert, M., & Ruiz, M. T. 2005, *ApJ*, 634, 1056
- Peimbert M. & Costero, R. 1969, *Bol. Obs. Tonantzintla y Tacubaya*, 5, 3
- Peimbert, M., Torres-Peimbert, S., & Ruiz, M.T. 1992, *Rev. Mex. Astron. Astrofís.*, 24, 155
- Peimbert, M., Peimbert, A., & Ruiz, M.T. 2000, *ApJ*, 541, 688
- Peimbert, M., Peimbert, A., Esteban, C., García-Rojas, J., Bresolin, F., Carigi, L., Ruiz, M. T., & López-Sánchez, A. R. 2007, *Revista Mexicana de Astronomía y Astrofísica Conference Series*, 29, 72
- Pérez-Montero, E., & Díaz, A. I. 2003, *MNRAS*, 346, 105
- Pilyugin, L. S., Vílchez, J. M., & Thuan, T. X. 2006, *MNRAS*, 370, 1928
- Porter, R. L., Bauman, R. P., Ferland, G. J., & MacAdam, K. B. 2005, *ApJ*, 622, L73
- Porter, R. L., Ferland, G. J., & MacAdam, K. B. 2007, *ApJ*, 657, 327

- Rayo, J. F., Peimbert, M., & Torres-Peimbert, S. 1982, *ApJ*, 255, 1
- Quinet, P. 1996, *A&AS*, 116, 573
- Rodríguez, M. 1999, *A&A*, 348, 222
- Rodríguez, M. & Rubin, R.H. 2005, *ApJ*, 626, 900
- Rosolowsky, E., & Simon, J. D. 2008, *ApJ*, 675, 1213
- Ruiz, M. T., Peimbert, A., Peimbert, M., & Esteban, C. 2003, *ApJ*, 595, 247
- Sakai, S., Ferrarese, L., Kennicutt, R. C., Jr., & Saha, A. 2004, *ApJ*, 608, 42
- Salzer, J. J., Lee, J. C., Melbourne, J., Hinz, J. L., Alonso-Herrero, A., & Jangren, A. 2005, *ApJ*, 624, 661
- Sawey, P. M. J., & Berrington, K. A. 1993, *Atomic Data and Nuclear Data Tables*, 55, 81
- Seaton, M. J., 1979, *MNRAS*, 187, 73
- Shaw, R. A., & Dufour, R. J. 1995, *PASP*, 107, 896
- Smith, L.F., Shara, M.M. & Moffat, A.F.J. 1996, *MNRAS*, 281, 163
- Stasińska, G. 1978, *A&A*, 66, 257
- Stasińska, G. 1990, *A&AS*, 83, 501
- Stasińska, G. 2005, *A&A*, 434, 507
- Stasińska, G., Tenorio-Tagle, G., Rodríguez, M., & Henney, W. J. 2007, *A&A*, 471, 193
- Storey, P. J. 1994, *A&A*, 282, 999
- Storey, P. J., & Hummer, D. G. 1995, *MNRAS*, 272, 41
- Torres-Peimbert, S., Peimbert, M., & Fierro, J. 1989, *ApJ*, 345, 186
- Tsamis, Y. G., Barlow, M. J., Liu, X.-W., Danziger, I. J., & Storey, P. J. 2003, *MNRAS*, 338, 687
- Tsamis, Y. G., & Péquignot, D. 2005, *MNRAS*, 364, 687
- Urbaneja, M. A., Herrero, A., Kudritzki, R.-P., Najarro, F., Smartt, S. J., Puls, J., Lennon, D. J., & Corral, L. J. 2005, *ApJ*, 635, 311

- van Zee, L., Salzer, J. J., Haynes, M. P., O'Donoghue, A. A., & Balonek, T. J. 1998, *AJ*, 116, 2805
- Verner, E.M., Verner, D.A., Baldwin, J.A., Ferland, G.J. & Martin, P.G. 2000, *ApJ*, 543, 831
- Véron, P., & Sauvayre, A. 1965, *Annales d'Astrophysique*, 28, 698
- Vílchez, J. M., Pagel, B. E. J., Diaz, A. I., Terlevich, E., & Edmunds, M. G. 1988, *MNRAS*, 235, 633
- Vogt, S. S., et al. 1994, *Proc. SPIE*, 2198, 362
- Walterbos, R. A. M., & Braun, R. 1992, *A&AS*, 92, 625
- Zaritsky, D., Elston, R., & Hill, J. M. 1989, *AJ*, 97, 97
- Zaritsky, D., Kennicutt, R. C., Jr., & Huchra, J. P. 1994, *ApJ*, 420, 87
- Zhang, H. L. 1996, *A&AS*, 119, 523
- Zhang, H. L., & Pradhan, A. K. 1997, *A&AS*, 126, 373

Table 10. Abundance Gradients in M33, M101, NGC 2403, and the Milky Way

Galaxy	O/H (CELs)	O/H (RLs)	C/H	C/O (RLs)
With respect to R_G^a				
M 33	-0.056 ± 0.029	-0.072 ± 0.047	-0.105 ± 0.120	-0.033 ± 0.130
M 101	-0.022 ± 0.004	-0.017 ± 0.009	-0.046 ± 0.012	-0.029 ± 0.020
NGC 2403	$+0.012 \pm 0.021$...	-0.097 ± 0.127	...
Milky Way ^b	-0.040 ± 0.006	-0.044 ± 0.010	-0.103 ± 0.018	-0.059 ± 0.020
With respect to R_0^c				
M 33	-0.39 ± 0.20	-0.50 ± 0.32	-0.72 ± 0.83	-0.22 ± 0.98
M 101	-0.62 ± 0.10	-0.50 ± 0.25	-1.32 ± 0.33	-0.65 ± 0.49
NGC 2403	$+0.09 \pm 0.17$...	-0.77 ± 1.00	...

^aIn units of dex kpc^{-1} .

^bEsteban et al (2005).

^cIn units of dex R_0^{-1} .